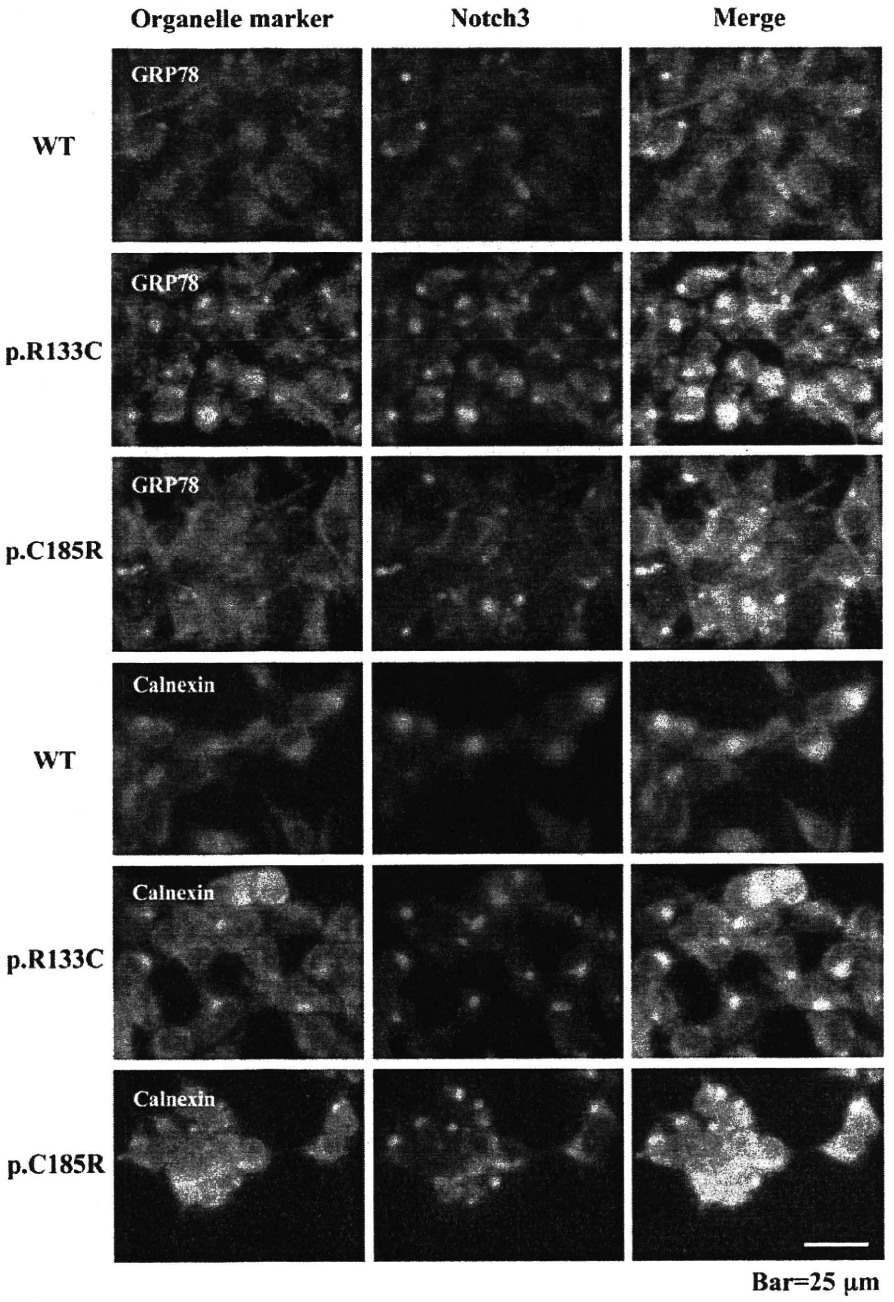

Figure 3. Subcellular localization of Notch3 aggregates. Stable cells expressing wild-type Notch3 (WT) or mutant Notch3 (p.R133C and p.C185R) were treated with tetracycline for 24 h. The cells were fixed and double-stained with antibodies. Organelle markers, GRP78/BiP and calnexin (green), were detected using primary antibodies, respectively, and visualized with either an Alexa Fluor 488-labeled secondary antibody or an FITC-labeled secondary antibody (left panels). Notch3 (red) was detected using AbN2 developed with either a Rhodamine Red-labeled secondary antibody or a Cy3-labeled secondary antibody (middle panels). The right panels represent the overlay (merge). Most of the aggregates were colocalized with GRP78/BiP and calnexin. These data shown are from representative experiments using WT-2, p.R133C-63 and p.C185R-64 cell lines for GRP78/BiP and WT-78, p.R133C-38, p.C185R-23 cell lines for calnexin, respectively. Scale bar, 25 μm.

profile as assessed by cell counting over a variable period lasting from 1 to 5 days. Expression of mutant Notch3 in tetracycline-treated cells decreased the cell number compared with that in untreated cells, whereas expression of wild-type Notch3 had relatively little overall effect on cell growth. The growth rates of cells expressing mutant Notch3 were not improved after turning off the expression of mutant Notch3 by removing tetracycline treatment (data not shown).

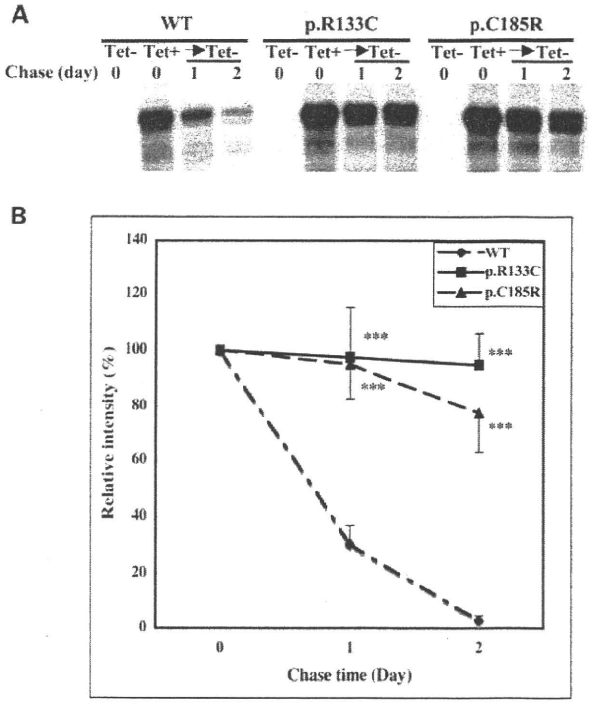

Figure 4. Efficiency and kinetics of Notch3 degradation. (**A**) Cells were treated with 2 μg/ml tetracycline for 24 h and then pulse-labeled for 2 h with L-[^{35}S]methionine and L-[^{35}S] cysteine. The labeled protein was chased for the indicated times by incubation in normal medium and then immunoprecipitated with an anti-Notch3 antibody (AbN2). The immunoprecipitates were separated on an acrylamide gel and visualized by autoradiography. The data shown are from one representative experiment for three stable cell lines (WT-2, p.R133C-3 and p.C185R-16). The experiment was performed twice using six stable cell lines (WT-2, WT-85, p.R133C-3, p.R133C-38, p.C185R-16 and p.C185R-23) and similar results were obtained. (**B**) Densitometric analysis of the autoradiograms was performed to estimate the relative amounts of wild-type Notch3 and mutant Notch3. Wild-type Notch3 rapidly disappeared within 2 days, whereas most of mutant Notch3 were still detectable after 2 days. Results represent means ± SD of data from two labeling experiments and are shown as the percentage of the material present at time 0. $^{***}P < 0.0001$ relative to wild-type Notch3.

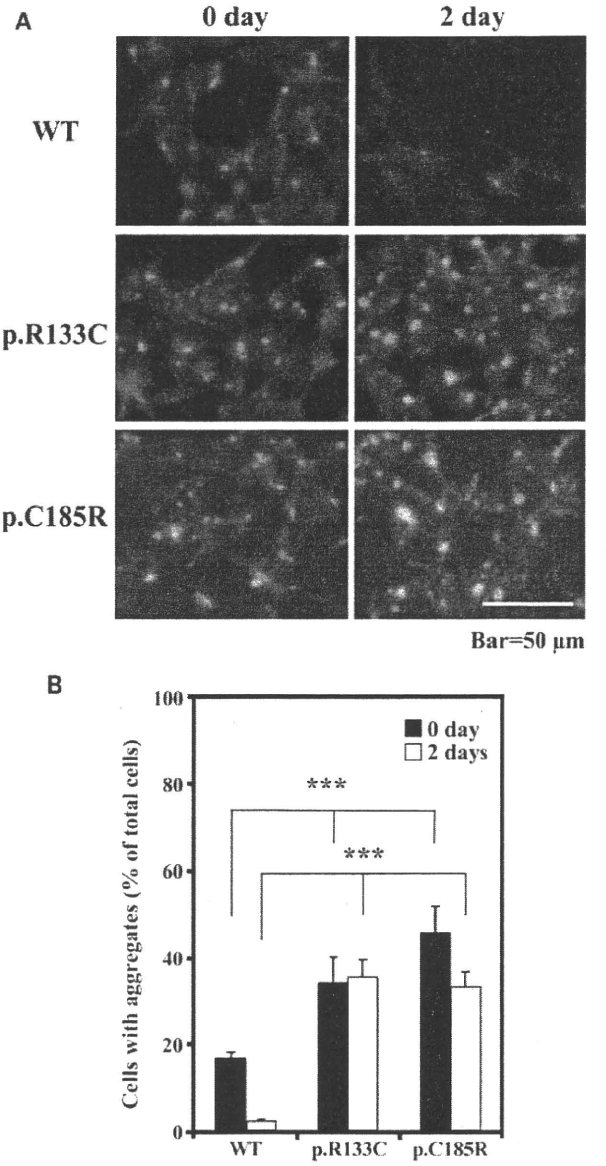

Figure 5. Retention and clearance of aggregates in cells expressing wild-type Notch3 and mutant Notch3. Cells were treated with 2 μg/ml tetracycline for 24 h and then incubated in medium without tetracycline for 2 days. (**A**) Cells were fixed at the time indicated and stained with an anti-Notch3 antibody (AbN2). The data shown represent one experiment for three stable cell lines (WT-78, p.R133C-63 and p.C185R-16). The experiment was performed twice using nine stable cell lines and similar results were obtained. Scale bar, 50 μm. (**B**) Cells with aggregates were quantified manually by counting cell numbers at the indicated times after removing tetracycline (0 days and 2 days). The aggregates of wild-type Notch3 quickly disappeared, whereas mutant aggregates did not show any discernible reduction up to 2 days. Results represent means ± SD of data from four independent images of each stable cell and are shown as the percentage of total cells counted. $^{***}P < 0.0001$ relative to wild-type Notch3-expressing cells.

These results were also confirmed in a cell proliferation assay using the WST-1 reagent (Fig. 7B and C). After 3 days of tetracycline treatment, stable cells expressing wild-type Notch3 were nearly 100% viable compared with the untreated cells, whereas cells expressing the mutant Notch3 exhibited significantly decreased viability at 33.2 and 37.8% for p.R133C and p.C185R, respectively (Fig. 7C). However, the cells expressing mutant Notch3 proteins reached confluence and did not exhibit any detectable apoptosis or other morphological abnormalities. These results suggest that expression of mutant Notch3 or aggregate accumulation decreases cell proliferation rates.

Inhibition of proteasome function increased cell death in cells expressing mutant Notch3

To determine whether apoptosis induced by impaired proteasome function depends on mutant Notch3, cell lines were treated with the proteasome inhibitor MG132 (3 μM), and cell viability was analyzed using the WST-1 assay. As shown in Figure 8A, the cells expressing mutant Notch3 were markedly sensitive to proteasome inhibition, and cell

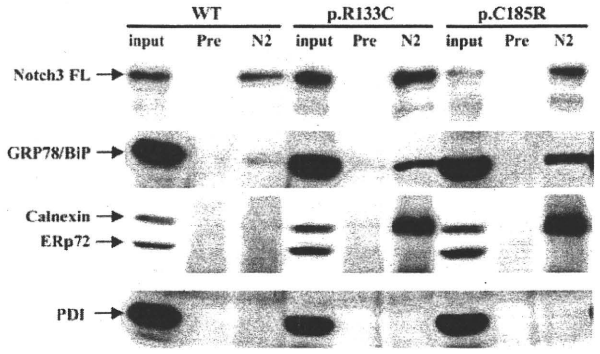

Figure 6. Identification of ER chaperones associated with mutant Notch3 by western blot analysis. Cell lysates were prepared from stable cells expressing either wild-type Notch3 or mutant Notch3 (p.R133C and p.C185R). Cell lysates (200 μg) were subjected to immunoprecipitation using an anti-Notch3 antibody (AbN2) or preimmune rabbit IgG (Pre). Immunoprecipitated complexes were subjected to SDS–PAGE, and western blot analysis was performed using mouse monoclonal antibodies against Notch3 (3A2), GRP78/BiP, calnexin, ERp72 and PDI. Total lysates (30 μg) were used as a positive control (input). The same membrane was probed simultaneously with Calnexin and ERp72 antibodies. Calnexin co-immunoprecipitated with mutant Notch3 but not with wild-type Notch3. In contrast, GRP78/BiP co-immunoprecipitated with both the wild-type and mutant Notch3. The data shown are from one representative experiment for three stable cell lines (WT-2, p.R133C-38 and p.C185R-63). The experiments were performed twice for each stable cell line with identical results.

viability was decreased by about 50% in tetracycline-treated cells compared with untreated cells. In cells expressing wild-type Notch3, there were no apparent differences in viability between tetracycline-treated and untreated cells. The effects of MG132 on cell viability are summarized in Figure 8B. These results strongly implicate that proteasome inhibition resulted in cytotoxicity associated with the accumulation of mutant Notch3.

DISCUSSION

In this study, we have shown that mutant Notch3 is more prone to form aggregates than wild-type Notch3 and that the mutant aggregates are resistant to degradation, leading to their accumulation in the ER at least in stably transfected HEK cells. The prolonged ER retention of mutant aggregates also impairs cell proliferation. A previous study reported that mouse mutant Notch3 gives rise to the increased numbers of intracellular aggregates, although the aggregates were apparently not colocalized with the markers for the ER, Golgi complex or the intermediate compartment (16). It is plausible that the modified Notch3 clone used in this study comprising chimeric receptors with insertion of the Gal4VP16 domain in the C-terminal region affected the subcellular localization of mutant Notch3. In addition, we showed that cells expressing mutant Notch3 exhibit increased sensitivity to the proteasome inhibitor MG132 resulting in cell death, which indicates that an additional stressor may be induced to disrupt cellular function. These findings suggest that impairment of ER function caused by the retention of mutant Notch3 is involved in the pathogenesis of CADASIL.

Excessive protein loading in the ER such as overexpression of either membrane proteins or secretory proteins usually induces the UPR, which is responsible for transcriptional attenuation of protein synthesis, upregulation of ER chaperones and folding enzymes to increase the capacity of the ER for protein folding and degradation (22–28). Mutations also cause aberrant folding and accumulation of the mutant protein in the ER. These unfolded proteins are retrotranslocated across the ER membrane and degraded by the ERAD process to relieve ER stress. However, some misfolded proteins are not degraded efficiently and are retained in the ER (29–33); a process which may be central to the pathogenesis of several diseases associated with ER stress. Our results showed that overexpression of wild-type Notch3 and mutant Notch3 induced the formation of aggregates in the ER, although the clearance rates of these proteins were markedly different. The aggregates of mutant Notch3 were retained in the ER and exhibited half-lives of longer than 6 days, but the aggregates of wild-type Notch3 disappeared with a half-life of less than a day. Thus, mutant Notch3 proteins form abnormal aggregates that appear trapped in the ER and are resistant to removal via the ERAD system. In contrast, the wild-type aggregates seem to be transiently formed and are readily susceptible to refolding and degradation. The biological properties that render mutant proteins prone to slower degradation remain to be identified. Because CADASIL mutations result in a free cysteine residue in the extracellular domain of Notch3, it is possible that aberrant disulfide-linking in mutant Notch3 increases the formation of aggregates and impairs the interaction with ER chaperones and proteases for efficient degradation. Recently, it has been reported that CADASIL-associated mutations significantly enhance Notch3 multimerization mediated by disulfide bonds compared with wild-type Notch3 (34). The structure of mutant Notch3 aggregates, however, may potentially be distinguished from those of wild-type aggregates by resistance to degradation, because in our experiments, wild-type Notch3 was cleared within 2 days after arresting its expression. Our preliminary experiments also revealed that both wild-type Notch3 and mutant Notch3 can be precipitated by centrifugation of cell lysates at 105 000*g* for 1 h in the presence of 1% Triton X-100 (Supplementary Material, Fig. S3), indicating that Notch3 forms a detergent-insoluble complex with a higher molecular weight. Thus, other proteins associated with the large complexes may account for the prolonged ER retention and slower degradation of mutant Notch3.

The immunoprecipitation studies suggest that calnexin only interacts with mutant Notch3. Calnexin functions as a lectin interacting with monoglucosylated oligosaccharides in folding intermediates of glycoproteins (35). Recently, it has been reported that calnexin retains misfolded proteins in membranous bodies of the ER and attenuates their degradation by the ERAD pathway (36), and overexpression of calnexin impedes trafficking of the dopamine receptor (37). Therefore, the specific interaction of mutant Notch3 with calnexin could account for the ER retention and the slower turnover rate of mutant proteins. On the other hand, CADASIL mutations have been reported to impair glycosylation of the truncated forms of Notch3 by Fringe and may induce aberrant dimerization (38). The glycosylation defects in mutant Notch3 might

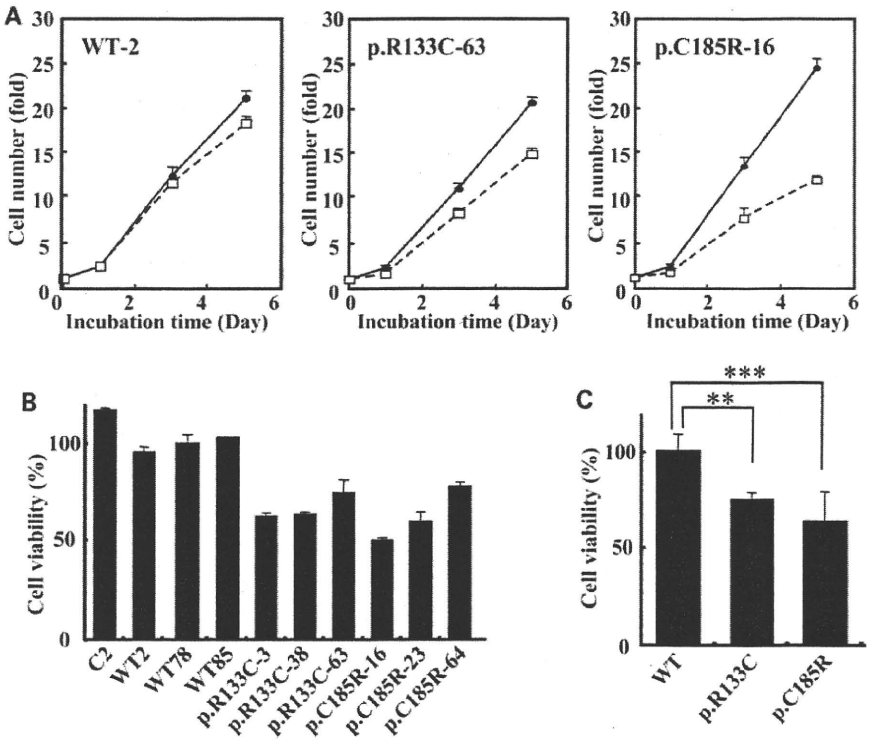

Figure 7. Comparison of proliferation rate in cells expressing either wild-type Notch3 or mutant Notch3. (**A**) Cells were incubated with (open squares) or without (closed circles) tetracycline and then harvested on days 0, 1, 3 and 5 for each of the three stable cell lines (WT-2, p.R133C-63 and p.C185R-16). Expression of mutant Notch3 decreased the cell number, whereas expression of wild-type Notch3 had relatively little overall effect on cell growth. Each data point represents the number of mean cells ± SD for triplicate counts as described in Materials and Methods. (**B**) Stable cells were incubated with or without tetracycline for 3 days. Cell viability was determined using the WST-1 reagent. C2 indicates the stable cell line transfected with empty vectors. Results represent means ± SD for triplicate wells and are shown as the percentage of the total number of cells without tetracycline treatment. (**C**) Cell viability for each cell line was converted to a percentage of the mean value relative to that of wild-type-expressing cells. Stable cells expressing wild-type Notch3 were nearly 100% viable compared with the untreated cells, whereas cells expressing the mutant Notch3 exhibited significantly decreased viability. Results represent the means ± SD of the data from different groups of cell lines (wild-type, $n = 5$; p.R133C mutant, $n = 4$; p.C185R mutant, $n = 4$). $^{**}P < 0.01$ and $^{***}P < 0.001$ relative to wild-type Notch3-expressing cells.

increase its binding affinity to calnexin compared with wild-type Notch3.

Proteasome function is essential for normal ERAD, and its inhibition causes accumulation of misfolded proteins in the ER and activates apoptotic pathways leading to cell death (39–42). Our study demonstrated that treatment with the proteasome inhibitor MG132 promoted cell death in cells expressing mutant Notch3, although cell death in cultures was not directly induced by expression of wild-type and mutant Notch3. These findings suggest that an additive effect caused by proteasome inhibition might induce apoptosis of cells with enhanced protein accumulation in the ER. It is conceivable that cells expressing mutant Notch3 develop increased sensitivity to other stress inducers such as hypoxia, oxidative stress and glucose deprivation (43–45), all of which may involve proteasome dysfunction.

Our results suggest that the cytotoxic effects of mutant Notch3 are due to its aggregate-prone property and resistance to degradation. Because all of the present experiments were performed with cultured HEK293 cells, we cannot readily extend our conclusions to *in vivo* effects of the mutation on VSMCs; however, our findings have important implications for our understanding of CADASIL pathology. First, the formation of GOM may be facilitated by the propensity for aggregation of mutant Notch3 because the extracellular domain of mutant Notch3 is a major component of GOM (8). As GOM deposits are detected around degenerating VSMCs or in the indentations of these cells, but not within the cells, it is possible that its formation occurs on the cell surface, where mutant Notch3 might act as a seed to recruit other proteins for the formation of large aggregates. It is also plausible that GOM deposits are formed in the ER and released in the extracellular space by the degeneration and disruption of VSMCs. Second, several proteins involved in protein folding and degradation have been recently reported to be upregulated in cultivated CADASIL VSMCs, suggesting that the expression of mutant Notch3 induces the UPR or impairs ERAD (21). Furthermore, disturbances in the cell surface involving cell adhesion or cell–matrix interactions might be due to impaired synthesis and transport of key membrane proteins caused by the insufficient ERAD of mutant Notch3 (20).

In summary, our study demonstrated that the intrinsic properties of mutant Notch3, which tend to form aggregates that

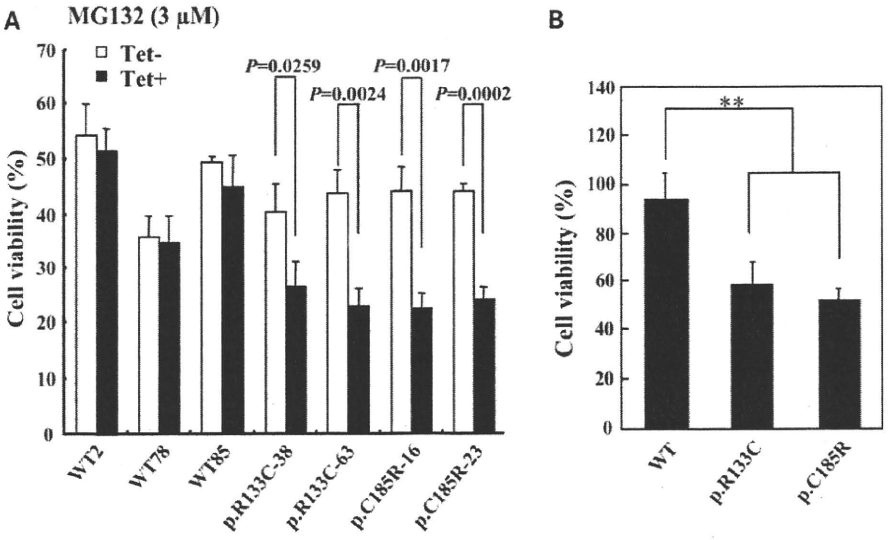

Figure 8. Different levels of sensitivity to a proteasome inhibitor. Stable cells were treated for 24 h with 3 μM MG132 in the presence (Tet+) or absence (Tet−) of tetracycline. Cell viability was determined using WST-1 reagent. (**A**) Results represent means ± SD for triplicate wells and show the percentage of the total number of cells not treated with MG132. The experiment was repeated three times using seven stable cell lines, with similar results each time. (**B**) Cell viability is summarized for cells expressing wild-type Notch3, R133C mutant Notch3 and C185R mutant Notch3, respectively. After treatment with MG132, cells expressing mutant Notch3 (Tet+) exhibited lower cell viability compared with cells not expressing Notch3 (Tet−), but cell viability was not affected by the expression of wild-type Notch3. The *y*-axis shows the percentage of the Tet+ cells to the Tet− cells exposed to MG132. Results represent means ± SD of the data. ** $P < 0.001$ relative to wild-type Notch3-expressing cells.

are resistant to the ERAD system, cause toxic effects on the proliferation of cultured cells. Further studies will be necessary to investigate the formation of mutant Notch3 aggregates in animal models and to assess their cytotoxic effects in VSMCs. Nevertheless, our findings raise the possibility that agents that inhibit the aggregation or enhance clearance of mutant Notch3 will become targets for the effective treatment or alleviation of CADASIL.

MATERIALS AND METHODS

Stable cell lines

HEK293 cells were grown in DMEM containing 10% fetal bovine serum and antibiotics. Human Notch3 cDNA (nucleotide numbers, -60-7375) was isolated from a human fetal brain cDNA library. The influenza hemagglutinin tag sequence was inserted in frame at the 3′ end of the coding region of the Notch3 cDNA. Two CADASIL mutations (p.R133C and p.C185R) in the EGF repeats were induced using a site-directed mutagenesis kit (Stratagene). The cDNAs of wild-type Notch3 and two Notch3 mutants were cloned into the *Xba*I and *Nhe*I sites of a pcDNA4/TO vector (Invitrogen) to regulate Notch3 expression using the T-Rex system (Invitrogen). All constructs were co-transfected into HEK293 cells with pcDNA/TR6 (Invitrogen) at a 1:1 ratio using an Effectene kit (Qiagen). After 48 h, cells were selected in the presence of 300 mg/ml Zeocin and 15 μg/ml blasticidin-S (Invitrogen). The expression level of Notch3 was determined by western blot analysis using an anti-Notch3 antibody (AbN2) after treatment with tetracycline (Tet; 2 μg/ml) for 48 h. The stable cell lines were maintained in DMEM containing 10% fetal bovine serum, 200 μg/ml Zeocin and 10 μg/ml blasticidin-S. The C2 clone was the stable cell line transfected with empty vectors.

Preparation of anti-Notch3 antibodies

Two rabbit polyclonal anti-human Notch3 antibodies (AbN2 and AbC2) were raised against glutathione-*S*-transferase fusion proteins containing amino acid residues 1497–1624 and 2261–2321 from the human Notch3, respectively (19). Monoclonal antibody 3A2 was raised against a synthetic peptide containing amino acid residues 1524–1538.

Western blot analysis

Cells were harvested and lysed in solution A containing 1% Triton X-100, 0.1 M Tris–HCl, pH 7.4, 0.15 M NaCl and a protease inhibitor cocktail (Boehringer Mannheim) as previously described (19). Lysates (30 μg/lane) were separated on a 7–10% SDS gel, and the separated proteins were transferred to a nitrocellulose membrane (Bio-Rad). The membrane was blocked in TBST (10 mM Tris–HCl, pH 7.4, 150 mM NaCl, 0.1% Tween-20) containing 5% non-fat milk and probed with the primary antibodies namely anti-human Notch3 (AbN2 and AbC2), anti-GAPDH (Sigma) and mouse monoclonal antibodies in a Chaperone Sampler kit (BD Biosciences), including anti-GRP78/BiP, anti-calnexin, anti-ERp72 and anti-PDI (protein disulfide isomerase). Immunoreactive proteins were detected by Western Lightning chemiluminescence reagents (Perkin Elmer). Protein concentrations were determined using the micro-BCA assay (Pierce).

Immunocytochemistry

Cells were cultured in 35 mm Petri dishes coated with poly-L-lysine and fixed in 4% paraformaldehyde in PBS at 4°C for 10 min. After treatment with 0.2% Triton X-100 for 10 min, cells were blocked with PBS containing 3% fetal bovine serum for 30 min and incubated for 1 h with the following primary antibodies at room temperature: a rabbit anti-human Notch3 (AbN2) (1 μg/ml), a goat anti-GRP78/BiP (C-20) antibody (Santa Cruz Biotechnology, diluted 1:100), a mouse anti-calnexin antibody (BD Biosciences, diluted 1:100) and a mouse anti-Golgi 58K protein antibody (Sigma, diluted 1:100). For the negative control, we used normal IgG instead of the primary antibody. Cells were washed three times with PBS and incubated for 1 h with the appropriate secondary antibodies including an Alexa Fluor 488-labeled goat anti-mouse antibody, a Rhodamine Red-labeled goat anti-rabbit antibody (Molecular Probes), an FITC-labeled donkey anti-goat antibody and a Cy3-labeled donkey anti-rabbit antibody (Chemicon) at a 1:1000 dilution in PBS. After three washes in PBS, cells were counterstained with DAPI (4′,6′-diamino-2-phenylindole, Molecular Probes) (5 μg/ml, 5 min), washed in PBS and examined under a light microscope (Olympus).

Pulse-chase analysis

Cells (1.2×10^6) were incubated for 24 h in 6-well plates coated with poly-L-lysine and treated with 2 μg/ml tetracycline for 24 h. The cells were then starved for 3 h in cysteine/methionine-free DMEM (Invitrogen) supplemented with 1% L-glutamine and 10% dialyzed fetal bovine serum and labeled for 2 h by the addition of 0.1 mCi/ml Pro-Mix L-[^{35}S] *in vitro* labeling mix (GE Healthcare). The culture medium was changed to fresh medium containing cold cysteine and methionine and chased for the indicated times. At each time point, cells were harvested and lysed in solution A (described above). The cell lysates were immunoprecipitated with anti-Notch3 (AbN2), and immunocomplexes were subjected to SDS polyacrylamide gel electrophoresis as described above. The separated proteins were visualized by fluorography using the Amplify Fluorographic Reagent (GE Healthcare) and X-ray film (GE Healthcare).

Immunoprecipitation

Cells were harvested and lysed in solution A. The lysates (200 μg of protein) were precleared with a protein G-agarose bead slurry (Boehringer Mannheim) for 1 h at 4°C and incubated at 4°C for 24 h with 3 μl of AbN2 antibodies (1 mg/ml). Immunocomplexes were pulled down with protein G-agarose beads and washed three times with RIPA buffer (1% Triton X-100, 20 mM Tris–HCl, pH 7.5, 1% deoxycholate, 0.2% SDS, 0.15 M NaCl and a protease inhibitor cocktail). After addition of the gel loading solution with 10% β-mercaptoethanol and boiling for 3 min, samples were loaded on a 7% SDS–PAGE gel. Proteins were transferred to membranes and blotted with Notch3 and several chaperone proteins antibodies as described above. The immunoreactive proteins were detected by chemiluminescence as described above.

Comparison of cell proliferation rate

Stable cells (2×10^4) were seeded in the 24-well plates and treated with or without 2 μg/ml tetracycline for the indicated times at 0 (before treatment), 1, 3, 5 days (after treatment). To determine the numbers of proliferating cells at each time point and under each condition (with or without Tet), we separately harvested cells from three wells. Then, cells in each well were stained with Trypan Blue and counted four times. Data were obtained from three independent experiments, and a plot was expressed as the mean values ± SD ($n = 3$, from three wells).

Measurement of cell viability and induction of ER stress

Stable cells (5×10^5) were seeded in 6-well plates. After 24 h, cells were incubated in fresh medium containing 2 μg/ml tetracycline for 24 h and then harvested for western blot analysis. To assess cell growth rates, stable cells (2×10^4) were seeded in 24-well plates and treated with or without 2 μg/ml tetracycline for the indicated times. Cell growth was determined by two methods: by counting in Trypan Blue solution and by means of a cell proliferation assay using the WST-1 reagent (Cell proliferation assay kit, Chemicon). This kit was used for rapid and sensitive quantification of cell proliferation and viability. The assay is based on the cleavage of the tetrazolium salt WST-1 to formazan by cellular mitochondrial dehydrogenases. To assess the effect of the proteasome inhibitor MG132 (Calbiochem), cells (2×10^4) were seeded in 24-well plates coated with poly-L-lysine. After 24 h, cells were treated with MG132 (3 μM) for 24 h in the presence or absence of tetracycline, and cell viability was determined using the WST-1 reagent.

Statistical analysis

Data are presented as means ± SD. Statistical analysis was performed using unpaired *t*-test (two-tailed) or one-way ANOVA with Dunnett's multiple comparison post hoc test (PRISM version 5.0a; GraphPad Software, La Jolla, CA, USA). Values of $P < 0.05$ were considered significant.

SUPPLEMENTARY MATERIAL

Supplementary Material is available at *HMG* online.

ACKNOWLEDGEMENTS

We thank Ms Aki Nagasaki and Ms Mikiko Matsuzaki for excellent technical assistance.

Conflict of Interest statement. None declared.

FUNDING

This work was supported by the Program for Promotion of Fundamental Studies in Health Science of the National Institute of Biomedical Innovation (NIBIO), a Research Grant for Longevity Sciences (18C-4 to K.T.) from the Ministry of Health, Labour and Welfare and the Medical Research

Council, UK programme project (G0500247) on dementia after stroke.

REFERENCES

1. Tournier-Lasserve, E., Joutel, A., Melki, J., Weissenbach, J., Lathrop, G.M., Chabriat, H., Mas, J.L., Cabanis, E.A., Baudrimont, M., Maciazek, J. *et al.* (1993) Cerebral autosomal dominant arteriopathy with subcortical infarcts and leukoencephalopathy maps to chromosome 19q12. *Nat. Genet.*, **3**, 256–259.
2. Chabriat, H., Vahedi, K., Iba-Zizen, M.T., Joutel, A., Nibbio, A., Nagy, T.G., Krebs, M.O., Julien, J., Dubois, B., Ducrocq, X. *et al.* (1995) Clinical spectrum of CADASIL: a study of 7 families. Cerebral autosomal dominant arteriopathy with subcortical infarcts and leukoencephalopathy. *Lancet*, **346**, 934–939.
3. Ruchoux, M.M. and Maurage, C.A. (1997) CADASIL: Cerebral autosomal dominant arteriopathy with subcortical infarcts and leukoencephalopathy. *J. Neuropathol. Exp. Neurol.*, **56**, 947–964.
4. Dichgans, M., Mayer, M., Uttner, I., Brüning, R., Müller-Höcker, J., Rungger, G., Ebke, M., Klockgether, T. and Gasser, T. (1998) The phenotypic spectrum of CADASIL: clinical findings in 102 cases. *Ann. Neurol.*, **44**, 731–739.
5. Kalaria, R.N., Low, W.C., Oakley, A.E., Slade, J.Y., Ince, P.G., Morris, C.M. and Mizuno, T. (2002) CADASIL and genetics of cerebral ischaemia. *J. Neural. Transm. Suppl.*, **63**, 75–90.
6. Ruchoux, M.M., Chabriat, H., Bousser, M.G., Baudrimont, M. and Tournier-Lasserve, E. (1994) Presence of ultrastructural arterial lesions in muscle and skin vessels of patients with CADASIL. *Stroke*, **25**, 2291–2292.
7. Schröder, J.M., Sellhaus, B. and Jörg, J. (1995) Identification of the characteristic vascular changes in a sural nerve biopsy of a case with cerebral autosomal dominant arteriopathy with subcortical infarcts and leukoencephalopathy (CADASIL). *Acta Neuropathol.*, **89**, 116–121.
8. Ishiko, A., Shimizu, A., Nagata, E., Takahashi, K., Tabira, T. and Suzuki, N. (2006) Notch3 ectodomain is a major component of granular osmiophilic material (GOM) in CADASIL. *Acta Neuropathol.*, **112**, 333–339.
9. Joutel, A., Corpechot, C., Ducros, A., Vahedi, K., Chabriat, H., Mouton, P., Alamowitch, S., Domenga, V., Cécillion, M., Maréchal, E. *et al.* (1996) Notch3 mutations in CADASIL, a hereditary adult-onset condition causing stroke and dementia. *Nature*, **383**, 707–710.
10. Joutel, A., Vahedi, K., Corpechot, C., Troesch, A., Chabriat, H., Vayssière, C., Cruaud, C., Maciazek, J., Weissenbach, J., Bousser, M.G. *et al.* (1997) Strong clustering and stereotyped nature of Notch3 mutations in CADASIL patients. *Lancet*, **350**, 1511–1515.
11. Tikka, S., Mykkänen, K., Ruchoux, M.M., Bergholm, R., Junna, M., Pöyhönen, M., Yki-Järvinen, H., Joutel, A., Viitanen, M., Baumann, M. *et al.* (2009) Congruence between NOTCH3 mutations and GOM in 131 CADASIL patients. *Brain*, **132**, 933–939.
12. Joutel, A., Andreux, F., Gaulis, S., Domenga, V., Cécillon, M., Battail, N., Piga, N., Chapon, F., Godfrain, C. and Tournier-Lasserve, E. (2000) The ectodomain of the Notch3 receptor accumulates within the cerebrovasculature of CADASIL patients. *J. Clin. Invest.*, **105**, 597–605.
13. Artavanis-Tsakonas, S., Rand, M.D. and Lake, R.J. (1999) Notch signaling: cell fate control and signal integration in development. *Science*, **284**, 770–776.
14. De Strooper, B., Annaert, W., Cupers, P., Saftig, P., Craessaerts, K., Mumm, J.S., Schroeter, E.H., Schrijvers, V., Wolfe, M.S., Ray, W.J. *et al.* (1999) A presenilin-1-dependent γ-secretase-like protease mediates release of Notch intracellular domain. *Nature*, **398**, 518–522.
15. Struhl, G. and Adachi, A. (1998) Nuclear access and action of notch *in vivo*. *Cell*, **93**, 649–660.
16. Karlström, H., Beatus, P., Dannaeus, K., Chapman, G., Lendahl, U. and Lundkvist, J. (2002) A CADASIL-mutated Notch 3 receptor exhibits impaired intracellular trafficking and maturation but normal ligand-induced signaling. *Proc. Natl Acad. Sci. USA*, **99**, 17119–17124.
17. Peters, N., Opherk, C., Zacherle, S., Capell, A., Gempel, P. and Dichgans, M. (2004) CADASIL-associated Notch3 mutations have differential effects both on ligand binding and ligand-induced Notch3 receptor signaling through RBP-Jk. *Exp. Cell Res.*, **299**, 454–464.
18. Joutel, A., Monet, M., Domenga, V., Riant, F. and Tournier-Lasserve, E. (2004) Pathogenic mutations associated with cerebral autosomal dominant arteriopathy with subcortical infarcts and leukoencephalopathy differently affect Jagged1 binding and Notch3 activity via the RBP/Jk signaling pathway. *Am. J. Hum. Genet.*, **74**, 338–347.
19. Low, W.C., Santa, Y., Takahashi, K., Tabira, T. and Kalaria, R.N. (2006) CADASIL-causing mutations do not alter Notch3 receptor processing and activation. *Neuroreport*, **17**, 945–949.
20. Ruchoux, M.M., Domenga, V., Brulin, P., Maciazek, J., Limol, S., Tournier-Lasserve, E. and Joutel, A. (2003) Transgenic mice expressing mutant Notch3 develop vascular alterations characteristic of cerebral autosomal dominant arteriopathy with subcortical infarcts and leukoencephalopathy. *Am. J. Pathol.*, **162**, 329–342.
21. Ihalainen, S., Soliymani, R., Iivanainen, E., Mykkänen, K., Sainio, A., Pöyhönen, M., Elenius, K., Järveläinen, H., Viitanen, M., Kalimo, H. *et al.* (2007) Proteome analysis of cultivated vascular smooth muscle cells from a CADASIL patient. *Mol. Med.*, **13**, 305–314.
22. Ellgaard, L. and Helenius, A. (2003) Quality control in the endoplasmic reticulum. *Nat. Rev. Mol. Cell Biol.*, **4**, 181–191.
23. Kleizen, B. and Braakman, I. (2004) Protein folding and quality control in the endoplasmic reticulum. *Curr. Opin. Cel. Biol.*, **16**, 343–349.
24. Zhang, K. and Kaufman, R.J. (2006) The unfolded protein response: a stress signaling pathway critical for health and disease. *Neurology*, **66**, S102–S109.
25. Zhao, L. and Ackerman, S.L. (2006) Endoplasmic reticulum stress in health and disease. *Curr. Opin. Cell Biol.*, **18**, 444–452.
26. Yoshida, H. (2007) ER stress and diseases. *FEBS J.*, **274**, 630–658.
27. Ni, M. and Lee, A.S. (2007) ER chaperones in mammalian development and human diseases. *FEBS Lett.*, **581**, 3641–3651.
28. Calloni, G., Zoffoli, S., Stefani, M., Dobson, C.M. and Chiti, F. (2005) Investigating the effects of mutations on protein aggregation in the cell. *J. Biol. Chem.*, **280**, 10607–10613.
29. Bence, N.F., Sampat, R.M. and Kopito, R.R. (2001) Impairment of the ubiquitin-proteasome system by protein aggregation. *Science*, **292**, 1552–1555.
30. Tanaka, Y., Engelender, S., Igarashi, S., Rao, R.K., Wanner, T., Tanzi, R.E., Sawa, A., Dawson, V.L., Dawson, T.M. and Ross, C.A. (2001) Inducible expression of mutant α-synuclein decreases proteasome activity and increases sensitivity to mitochondria-dependent apoptosis. *Hum. Mol. Genet.*, **10**, 919–926.
31. Kaytor, M.D., Wilkinson, K.D. and Warren, S.T. (2004) Modulating huntingtin half-life alters polyglutamine-dependent aggregate formation and cell toxicity. *J. Neurochem.*, **89**, 962–973.
32. Ravikumar, B., Acevedo-Arozena, A., Imarisio, S., Berger, Z., Vacher, C., O'Kane, C.J., Brown, S.D.M. and Rubinsztein, D.C. (2005) Dynein mutations impair autophagic clearance of aggregate-prone proteins. *Nat. Genet.*, **37**, 771–776.
33. Fujita, E., Kouroku, Y., Isoai, A., Kumagai, H., Misutani, A., Matsuda, C., Hayashi, Y.K. and Momoi, T. (2007) Two endoplasmic reticulum-associated degradation (ERAD) systems for the novel variant of the mutant dysferlin: ubiquitin/proteasome ERAD(I) and autophagy/lysosome ERAD(II). *Hum. Mol. Genet.*, **16**, 618–629.
34. Opherk, C., Duering, M., Peters, N., Karpinska, A., Rosner, S., Schneider, E., Bader, B., Giese, A. and Dichgans, M. (2009) CADASIL mutations enhance spontaneous multimerization of NOTCH3. *Hum. Mol. Genet.*, **18**, 2761–2767.
35. Trombetta, E.S. and Parodi, A.J. (2003) Quality control and protein folding in the secretory pathway. *Annu. Rev. Cell Dev. Biol.*, **19**, 649–676.
36. Okiyoneda, T., Harada, K., Takeya, M., Yamahira, K., Wada, I., Shuto, T., Suico, M.A., Hashimoto, Y. and Kai, H. (2004) Delta F508 CFTR pool in the endoplasmic reticulum is increased by calnexin overexpression. *Mol. Biol. Cell*, **15**, 563–574.
37. Free, R.B., Hazelwood, L.A., Cabrera, D.M., Spalding, H.N., Namkung, Y., Rankin, M.L. and Sibley, D.R. (2007) D1 and D2 dopamine receptor expression is regulated by direct interaction with the chaperone protein calnexin. *J. Biol. Chem.*, **282**, 21285–21300.
38. Arboleda-Velasquez, J.F., Rampal, R., Fung, E., Darland, D.C., Liu, M., Martinez, M.C., Donahue, C.P., Navarro-Gonzalez, M.F., Libby, P., D'Amore, P.A. *et al.* (2005) CADASIL mutations impair Notch3 glycosylation by Fringe. *Hum. Mol. Genet.*, **14**, 1631–1639.

THE JOURNAL OF BIOLOGICAL CHEMISTRY VOL. 284, NO. 46, pp. 31914–31920, November 13, 2009

Aβ42-to-Aβ40- and Angiotensin-converting Activities in Different Domains of Angiotensin-converting Enzyme*

Received for publication, April 21, 2009, and in revised form, September 3, 2009 Published, JBC Papers in Press, September 22, 2009, DOI 10.1074/jbc.M109.011437

Kun Zou[‡1], Tomoji Maeda[‡], Atsushi Watanabe[§], Junjun Liu[‡], Shuyu Liu[‡], Ryutaro Oba[¶], Yoh-ichi Satoh[‖], Hiroto Komano[‡2], and Makoto Michikawa[3]**

*From the [‡]Department of Neuroscience, School of Pharmacy, and the [‖]Department of Anatomy, School of Medicine, Iwate Medical University, 2-1-1 Nishitokuda, Yahaba, Iwate 028-3694, Japan, the [¶]Department of Advanced Medicine and Development, BML, Inc., 1361-1 Matoba, Kawagoe, Saitama 350-1101, Japan, and the Departments of [§]Vascular Dementia Research and **Alzheimer Disease Research, National Institute for Longevity Sciences, National Center for Geriatrics and Gerontology, 36-3 Gengo, Morioka, Obu, Aichi 474-8522, Japan*

Amyloid β-protein 1–42 (Aβ42) is believed to play a causative role in the development of Alzheimer disease (AD), although it is a minor part of Aβ. In contrast, Aβ40 is the predominant secreted form of Aβ and recent studies have suggested that Aβ40 has neuroprotective effects and inhibits amyloid deposition. We have reported that angiotensin-converting enzyme (ACE) converts Aβ42 to Aβ40, and its inhibition enhances brain Aβ42 deposition (Zou, K., Yamaguchi, H., Akatsu, H., Sakamoto, T., Ko, M., Mizoguchi, K., Gong, J. S., Yu, W., Yamamoto, T., Kosaka, K., Yanagisawa, K., and Michikawa, M. (2007) *J. Neurosci.* 27, 8628–8635). ACE has two homologous domains, each having a functional active site. In the present study, we identified the domain of ACE, which is responsible for converting Aβ42 to Aβ40. Interestingly, Aβ42-to-Aβ40-converting activity is solely found in the N-domain of ACE and the angiotensin-converting activity is found predominantly in the C-domain of ACE. We also found that the *N*-linked glycosylation is essential for both Aβ42-to-Aβ40- and angiotensin-converting activities and that unglycosylated ACE rapidly degraded. The domain-specific converting activity of ACE suggests that ACE inhibitors could be designed to specifically target the angiotensin-converting C-domain, without inhibiting the Aβ42-to-Aβ40-converting activity of ACE or increasing neurotoxic Aβ42.

Angiotensin-converting enzyme (ACE)[4] plays a key role in the renin-angiotensin system (RAS), which is involved in the long-term regulation of blood pressure and blood volume in the human body. Recent genetic, pathologic, and biochemical studies have associated ACE with onset of Alzheimer disease (AD) (1, 2). The I allele of the *ACE* gene, which results in a reduced serum ACE level, has been demonstrated to be associated with AD (3–5). Hypertension is a risk factor for AD and ACE inhibitors for treatment of hypertension were shown to be the only drug class among the antihypertensives to potentially be associated with a slight increased incidence of AD (adjusted hazard ratio 1.13) (6, 7). A mechanistic link between ACE and AD was suggested when ACE was shown to degrade Aβ40 and Aβ42 (8, 9). Overexpression of Aβ40 in transgenic mice does not cause brain amyloid deposition, the major pathological hallmark of AD, whereas expression of Aβ42 is shown to be essential for amyloid deposition (10, 11). In addition, Aβ40 has an inhibitory effect on amyloid deposition *in vitro* and *in vivo* and has neuroprotective effects (12–14). These lines of evidence suggest that converting Aβ42 to Aβ40 may be a potential strategy for development of an AD therapy. In our previous study, we identified ACE as an Aβ42-to-Aβ40-converting (Aβ-converting) enzyme and showed that ACE inhibitor enhances brain Aβ42 deposition in transgenic mice (15). Clarifying the molecular base of ACE domain-specific enzymatic activity on Aβ42 to Aβ40 conversion, Aβ degradation, and angiotensin conversion emerges to be important for development of a strategy for hypertension and AD treatment.

ACE is a type I integral membrane glycoprotein, and there are two isoforms of ACE in mammals that arise from the use of alternative promoters in a single gene: somatic ACE and testicular ACE. ACE also has one mammalian relative, ACE2, which consists of a single active site domain that, by sequence comparison, more closely resembles the N-domain than the C-domain of somatic ACE. ACE converts angiotensin I to angiotensin II, a potent vasoconstrictor, and inactivates bradykinin, a vasodilator (16). Given the central role ACE plays in regulation of blood pressure, ACE inhibitors are widely used for the treatment of hypertension in the elderly population. ACE also hydrolyzes a wide range of polypeptide substrates, including substance P, luteinizing hormone-releasing hormone, acetyl-Ser-Asp-Lys-Pro (AcSDKP), and neurotensin (16). The mammalian somatic ACE contains two homologous domains, the N-terminal domain (N-domain) and C-terminal domain (C-domain), each bearing a zinc-dependent active site. The pres-

* This work was supported by grants from the Ministry of Education, Culture, Sports, Science and Technology of Japan, Grant-in-Aid for Young Scientists (Start-up) (19800040), and Scientific Research (B) (19300138), the Ministry of Health, Labor and Welfare of Japan (Comprehensive Research on Aging and Health) (H20-007), the Program for Promotion of Fundamental Studies in Health of the National Institute of Biomedical Innovation (NIBIO), Takeda Science Foundation, Kato Memorial Bioscience Foundation, and The Ichiro Kanehara Foundation for the Promotion of Medical Sciences and Medical Care.

[1] To whom correspondence may be addressed. Tel.: 81-19-698-1820; Fax: 81-19-698-1864; E-mail: kunzou@iwate-med.ac.jp.

[2] To whom correspondence may be addressed. Tel.: 81-19-698-1820; Fax: 81-19-698-1864; E-mail: hkomano@iwate-med.ac.jp.

[3] To whom correspondence may be addressed. Tel.: 81-562-46-2311; Fax: 81-562-46-8569; E-mail: michi@nils.go.jp.

[4] The abbreviations used are: ACE, angiotensin-converting enzyme; Aβ, amyloid β-protein; F-ACE, full-domain ACE; N-ACE, N-terminal domain ACE; C-ACE, C-terminal domain ACE; MALDI-TOF-MS, matrix-assisted laser desorption ionization-time of flight-mass spectrometry; AD, Alzheimer Disease.

39. Tsai, B., Ye, Y. and Rapoport, T.A. (2002) Retro-translocation of proteins from the endoplasmic reticulum into the cytosol. *Nat. Rev. Mol. Cell Biol.*, **3**, 246–255.
40. Friedman, J. and Xue, D. (2004) To live or die by the sword: the regulation of apoptosis by the proteasome. *Dev. Cell*, **6**, 460–461.
41. Mytilineou, C., McNaught, K.S., Shashidharan, P., Yabut, J., Baptiste, R.J., Parnandi, A. and Olanow, C.W. (2004) Inhibition of proteasome activity sensitizes dopamine neurons to protein alterations and oxidative stress. *J. Neural Transm.*, **111**, 1237–1251.
42. Bennett, E.J., Bence, N.F., Jayakumar, R. and Kopito, R.R. (2005) Global impairment of the ubiquitin-proteasome system by nuclear or cytoplasmic protein aggregates precedes inclusion body formation. *Mol. Cell*, **17**, 351–365.
43. Zinszner, H., Kuroda, M., Wang, X., Batchvarova, N., Lightfoot, R.T., Remotti, H., Stevens, J.L. and Ron, D. (1998) CHOP is implicated in programmed cell death in response to impaired function of the endoplasmic reticulum. *Genes. Dev.*, **12**, 982–995.
44. McCullough, K.D., Martindale, J.L., Klotz, L.O., Aw, T.Y. and Holbrook, N.J. (2001) Gadd153 sensitizes cells to endoplasmic reticulum stress by down-regulating Bcl2 and perturbing the cellular redox state. *Mol. Cell. Biol.*, **21**, 1249–1259.
45. Paschen, W. and Frandsen, A. (2001) Endoplasmic reticulum dysfunction—a common denominator for cell injury in acute and degenerative diseases of the brain? *J. Neurochem.*, **79**, 719–725.

ence of two active sites in ACE has stimulated many attempts to establish whether they differ in function. For example, AcSDKP, a peptide suggested to inhibit bone marrow maturation, is found to be preferentially cleaved by the N-domain of ACE *in vitro* (17). In contrast, the ACE C-domain is demonstrated to be the main site of angiotensin I cleavage *in vivo* (18). The *N*-linked glycosylation of testicular ACE, a homologue of the somatic ACE N-domain, is essential for its enzymatic activity and for preventing degradation (19).

In our current study, we determined the contributions of each ACE domain, toward Aβ42-to-Aβ40- and/or angiotensin-converting activity. We postulated that the dipeptidyl carboxypeptidase activity of ACE, which converts angiotensin I to angiotensin II and Aβ42 to Aβ40, is located in its C-domain. Surprisingly, we found that the Aβ42-to-Aβ40-converting activity is specifically in the N-domain of ACE, and the angiotensin-converting activity is predominantly in the C-domain of ACE. We also found that both Aβ42-to-Aβ40- and angiotensin-converting activities require the *N*-linked glycosylation of ACE. The finding of domain-specific Aβ42-to-Aβ40-converting activity of ACE may help design a domain-specific ACE inhibitor for treatment of hypertension, without inhibiting the N-domain-specific Aβ42-to-Aβ40-converting activity of ACE.

EXPERIMENTAL PROCEDURES

Truncated ACE Expression and Purification—Expression and purification of ACE recombinant proteins were carried out as described previously (20). Mutated ACE cDNAs containing two active domains (F-ACE) or only the N-terminal active domain or C-terminal active domain (N-ACE or C-ACE) were cloned into pcDNA3.1(-) vectors (Invitrogen). Six histidine residues were introduced at the C-terminal end of each cDNA. The C-terminal transmembrane domain was removed from all of the recombinant ACE proteins to allow them to be secreted into the culture medium. COS7 cells were grown in Dulbecco's modified Eagle's medium (DMEM) containing 10% fetal bovine serum. Transfections of the ACE pcDNA3.1(-) vectors in COS7 cells were performed using Lipofectamine 2000 (Invitrogen), and COS7 cells stably expressing F-, N-, and C-ACE were selected in DMEM containing 10% fetal bovine serum and 1 mg/ml Geneticin (Wako, Japan). Culture media were harvested 3 days after the cells reached confluence, and recombinant ACE proteins were purified using a TALON purification kit (Clontech). The purified proteins were then dialyzed in 50 mM HEPES, 50 mM NaCl, 1 μM $ZnCl_2$, pH 7.5 and concentrated with Centricon YM-50 (Millipore). Protein concentrations of the ACE proteins were determined using a BCA protein assay kit (Pierce).

Western Blot Analysis and Determining Conversion of Aβ42 to Aβ40—COS7 cells were lysed in radioimmune precipitation assay buffer (10 mM Tris/HCl (pH 7.5), 150 mM NaCl, 1% Nonidet P-40, 0.1% sodium dodecyl sulfate (SDS), and 0.2% sodium deoxycholate, containing a protease inhibitor mixture (Roche Applied Science)). The expression of ACE recombinant proteins was detected by Western blotting using a polyclonal anti-ACE antibody (R&D). Aβ1–42 (Peptide Institute) was freshly dissolved in 0.1% $NH_3 \cdot H_2O$ at 200 μM for each experiment. 80 μl of F-, N-, and C-ACE at a concentration of 0.5 μM were mixed with synthetic Aβ42 to a final concentration of 40 μM and incubated at 37 °C. 10 μl of the mixture was subjected to SDS-PAGE and blotted on a nitrocellulose membrane. To enhance the reactivity to an anti-Aβ40 antibody, the membrane was boiled in PBS for 3 min after blotting, probed with an anti-Aβ40 monoclonal antibody (1A10) (IBL), and visualized with SuperSignal (Pierce). Because of the high level of exogenous Aβ42, the membrane was not boiled before the reaction with a polyclonal anti-Aβ42 antibody. The quantitation of Aβ40 generation and Aβ42 degradation was carried out using Image J 1.41 software (NIH).

ACE Activity Assay—F-ACE, N-ACE, and C-ACE were dialyzed in 50 mM HEPES, 50 mM NaCl, 1 μM $ZnCl_2$, pH 7.5, and their activities against the synthetic substrate *N*-hippuryl-l-histidyl-l-leucine (Hip-His-Leu) were determined using an ACE colorimetric kit (Buhlmann Laboratories, Schonenbuch, Switzerland). 10 μl of ACE proteins at a concentration of 0.5 μM were mixed and incubated with ACE substrate at 37 °C. The reaction time was 15 min. All samples were measured in triplicate.

Mass Spectrometry Analysis—Purified F-ACE, N-ACE, or C-ACE was incubated with 80 μM Aβ42 at 37 °C for 2 h. Captopril (10 μM) was added to stop digestion, and the sample was frozen in −80 °C until use. The samples were mixed with 3,5-dimethoxy-4-hydroxycinnamic acid (Wako, Japan) as a matrix, and then subjected to matrix-assisted laser desorption ionization-time of flight-mass spectrometry (MALDI-TOF-MS) (AXIMA-CFR, SHIMADZU, Kyoto, Japan) to detect the generation of Aβ40 and other Aβ fragments. The same amount of F-ACE, N-ACE, C-ACE, or Aβ42 incubated alone under the same conditions as described above was used as control.

Expression of ACE Active Site Mutants and Determining Their Domain-specific Activities—The pcDNA5/FRT expression vectors bearing the catalytically inactive full-length ACE were kindly provided by Dr. Dennis J. Selkoe (9). The two ACE zinc metalloprotease active site glutamates (amino acids 362 in the N-domain and 960 in the C-domain) were changed to aspartates. Mouse embryonic fibroblasts at 90% confluence were transiently transfected with the vectors bearing ACE full-length protein with active site mutations using Lipofectamine 2000 (Invitrogen). After 48 h, the cells were lysed in in 50 mM Tris/HCl (pH 7.5) containing 0.5% Nonidet P-40, and nuclei and cell debris was pelleted at 10,000 × *g* for 10 min at 4 °C. To assay ACE activity, 5 μg of protein of cell lysate was incubated with Hip-His-Leu. For the Aβ42-to-Aβ40-converting activity assay, ACE in each cell lysate was immunoprecipitated using a polyclonal anti-ACE antibody (R&D) and protein G-Sepharose (GE Healthcare). Immunoprecipitated ACE was then incubated with 40 μM synthetic Aβ42 at 37 °C for 15 h. Captopril (10 μM) was added to the mixture to stop the reaction and the conversion of Aβ40 from Aβ42 was detected by Western blot.

Deglycosylation of ACE Proteins—To assess the type of glycosylation of human kidney ACE and recombinant ACE proteins, the ACE proteins were treated with PNGase F, *O*-glycanase, or sialidase A using an enzymatic deglycosylation kit according to the manufacturer's instructions (PROzyme, San Leandro, CA). To evaluate the enzymatic activities of deglycosylated ACE proteins, non-denaturing protocol was used, and ACE proteins

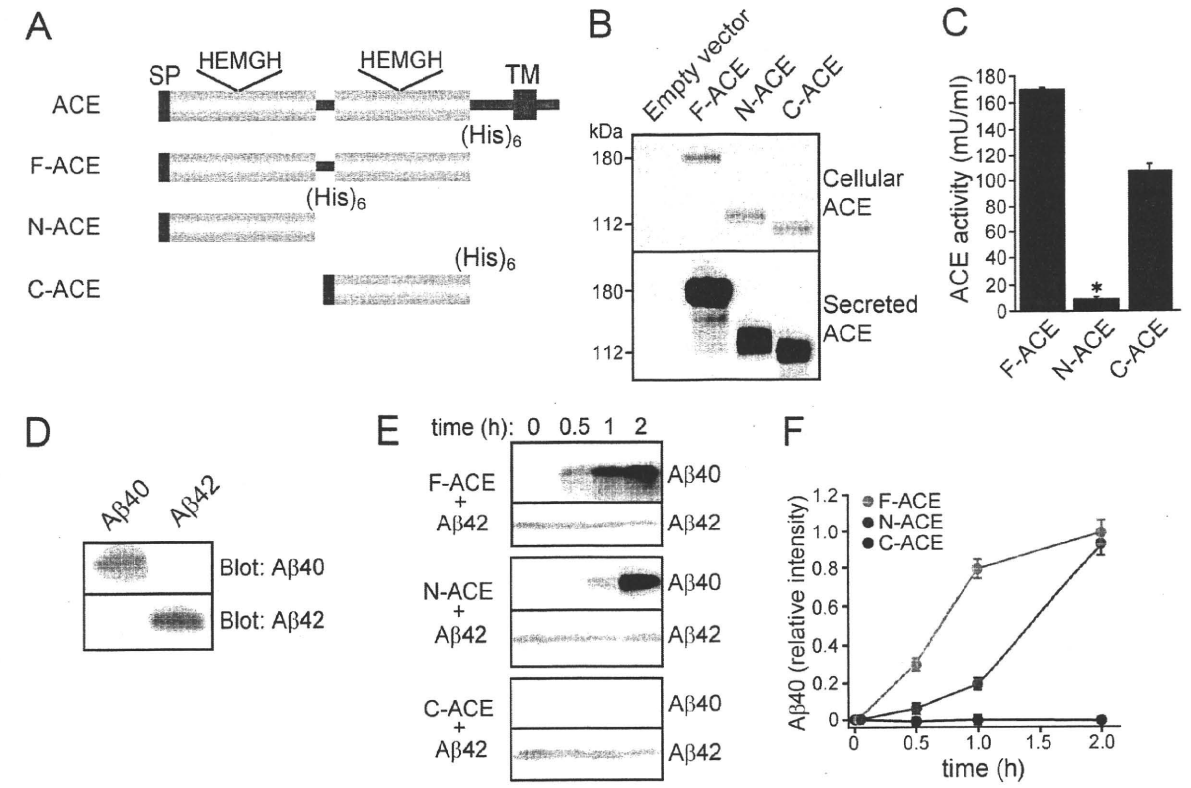

FIGURE 1. **Identification of N-domain-specific Aβ42-to-Aβ40-converting activity of ACE.** *A*, schematic representation of the human ACE and recombinant ACE proteins. The wild-type ACE protein contains a signal peptide (*SP*), a single transmembrane domain (*TM*), and two homologous catalytic domains (*light blue box*). Recombinant ACE proteins, F-ACE, N-ACE, and C-ACE, contain 6 histidine residues (*yellow box*) at the C terminus and a signal peptide at the N terminus. *B*, COS7 cells transfected with empty vector or cells stably expressing F-ACE, N-ACE, or C-ACE were lysed in radioimmune precipitation assay buffer. Western blots of 20 μg of total protein from the cells or 2 μg of ACE isolated from the culture medium were probed with a polyclonal anti-ACE antibody. *C*, ACE activity was measured by incubating 0.5 μM F-ACE, N-ACE, or C-ACE with the substrate Hip-His-Leu for 15 min at 37 °C. N-ACE has markedly reduced ACE activity compared with C-ACE. Values represent the means + S.E.; $n = 3$; *, $p < 0.001$, Bonferroni/Dunn test. *D*, specificities of monoclonal anti-Aβ40 (1A10) and polyclonal anti-Aβ42 antibodies were confirmed by Western blot of 0.1 μg of Aβ40 and Aβ42. *E*, F-, N-, and C-ACE were mixed with synthetic Aβ42 and incubated at 37 °C for 0.5, 1, or 2 h. Western blots of the mixture were probed with anti-Aβ40 and anti-Aβ42 antibodies. In contrast to the ACE activity, the Aβ42-to-Aβ40-converting activity was solely detected in N-ACE. *F*, generation of Aβ40 and the degradation of Aβ42 were determined by densitometry.

were deglycosylated at 37 °C for 1 h. The non-deglycosylated ACE proteins were mixed with the same incubation buffer provided by the manufacturer and incubated except that glycosidases were not added.

RESULTS

ACE N-domain, but Not C-domain, Converts Aβ42 to Aβ40—To explore which domain of ACE has Aβ42-to-Aβ40-converting activity, we prepared 3 kinds of recombinant ACE proteins, which were transfected into COS7 cells. F-ACE contains both the N-domain and C-domain active sites. N-ACE contains only the N-terminal active site, and C-ACE only contains the C-terminal active site. All three kinds of mutated ACE were fused with a 6-histidine tag at the C-terminal for the isolation from the culture medium (Fig. 1*A*). Cell lines stably expressing F-ACE, N-ACE, or C-ACE were selected by Geneticin and the expression of the ACE-mutated proteins were confirmed by Western blot. The endogenous ACE was not detected in the cell lysate of COS7 cells transfected with empty vectors. F-, N-, and C-ACE showed molecular masses at 180, 130, and 110 kDa, respectively (Fig. 1*B*). The secreted ACE recombinant proteins were isolated from the culture medium by immobilized metal chromatography. The proteins were then dialyzed and concentrated. The apparent molecular mass of each secreted ACE recombinant protein did not differ from each of the cellular ACE recombinant proteins (Fig. 1*B*). ACE enzymatic activity of the F-ACE, N-ACE, and C-ACE was confirmed by degradation of the substrate Hip-His-Leu (Fig. 1*C*). F-ACE was found to have the highest Hip-His-Leu-degrading activity and C-ACE had 63% ACE activity compared with F-ACE, whereas N-ACE had a significantly reduced ACE activity, confirming the finding of the ACE C-domain as the main site of angiotensin I cleavage *in vivo* (18) (Fig. 1*C*).

We have found that ACE releases two amino acids from the C terminus of Aβ42 and generates Aβ40. Aβ1–41 was not found during the degradation of Aβ42 by ACE, suggesting that the Aβ42-to-Aβ40-converting activity of ACE is a dipeptidyl carboxypeptidase enzymatic activity (15). To determine which domain is responsible for the Aβ42-to-Aβ40-converting activity, we incubated Aβ42 with F-ACE, N-ACE, or C-ACE and examined the generation of Aβ40 from Aβ42 by Western blot using anti-Aβ40- and anti-Aβ42-specific antibodies. The specificity of the two antibodies was examined by Western blotting of synthetic Aβ40 and Aβ42, and cross reaction between these

two antibodies was not found (Fig. 1*D*). Unexpectedly, in contrast to the angiotensin-converting activity, the Aβ42-to-Aβ40-converting activity was found in F-ACE and N-ACE, but not in C-ACE, indicating that N-domain of ACE has the Aβ42-to-Aβ40-converting activity. Although C-ACE showed a similar Aβ42-degrading activity compared with F-ACE and N-ACE, it did not generate Aβ40 from Aβ42 (Fig. 1*E*). Incubation of C-ACE with Aβ42 up until 16 h did not generate Aβ40 (data not shown). F-ACE generated more Aβ40 from Aβ42 than N-ACE at the time points of 0.5 and 1 h, whereas at the time point of 2 h F-ACE and N-ACE generated similar amounts of Aβ40 (Fig. 1, *E* and *F*). F-ACE had similar activities compared with native human kidney ACE regarding the Aβ42-to-Aβ40-converting activity and the Hip-His-Leu-degrading activity (Figs. 1*E* and 4*C* and data not shown).

To determine other products other than Aβ40 that were generated by ACE from Aβ42 and to confirm the result from Western blot, we performed mass spectrometry analysis. Consistent with our immunological studies, a peak corresponding to Aβ1–40 was detected in the F-ACE- and N-ACE-digested samples; in addition, F-ACE and N-ACE also generated peaks corresponding to Aβ1–33, Aβ1–28, Aβ1–24, and Aβ1–21 from Aβ42, whereas Aβ1–40 was not formed by C-ACE. However, C-ACE generated four other Aβ fragments, Aβ1–33, Aβ1–28, Aβ1–24, and Aβ1–21 (Fig. 2*A*). Mass spectrometry analysis for incubated F-ACE, N-ACE, or C-ACE alone did not show any Aβ peptide signal, and synthetic Aβ42 only showed one peak with a mass at 4514, which matched the predicted mass of Aβ1–42 (Fig. 2*B* and data not shown). These results from mass spectrometry confirmed that the Aβ42-to-Aβ40-converting activity is restricted to the ACE N-domain.

N-domain-inactive ACE Mutant Loses Aβ42-to-Aβ40-converting Activity—Three ACE mutants were generated by site-directed mutagenesis to change the active site sequence HEMGH to HDMGH in N-, C-, or both N- and C-domain. The N-domain active site was inactivated by mutating glutamate 362 to aspartate (termed E362D), and the C-domain active site was similarly inactivated by mutating glutamate 960 to aspartate (termed E960D). E362/960D has double mutations in its N- and C-domain active sites (Fig. 3*A*). The fibroblasts were transiently transfected with empty vector or ACE mutant constructs. ACE was not detected in the fibroblasts transfected with empty vector, and wtACE and ACE mutants were expressed in the cells at a similar level (Fig. 3*B*). To determine the effects of each ACE active site on ACE activity, cell lysate from each cell lines was analyzed for ACE activity. Consistent with our results from purified truncated ACE proteins, E362D containing only the C-domain active site has the similar ACE activity compared with wtACE, whereas E960D has an extremely low ACE activity. ACE inhibitor, captopril, completely inhibited this ACE activity (Fig. 3*C*). To determine which active site in each domain is responsible for the Aβ42-to-Aβ40-converting activity, wtACE and ACE mutant proteins were immunoprecipitated and incubated with Aβ42. A similar amount of immunoprecipitated ACE was confirmed by Western blotting (Fig. 3*D*, *upper panel*). E960D without the C-domain activity generated similar amount of Aβ40 from Aβ42 compared with

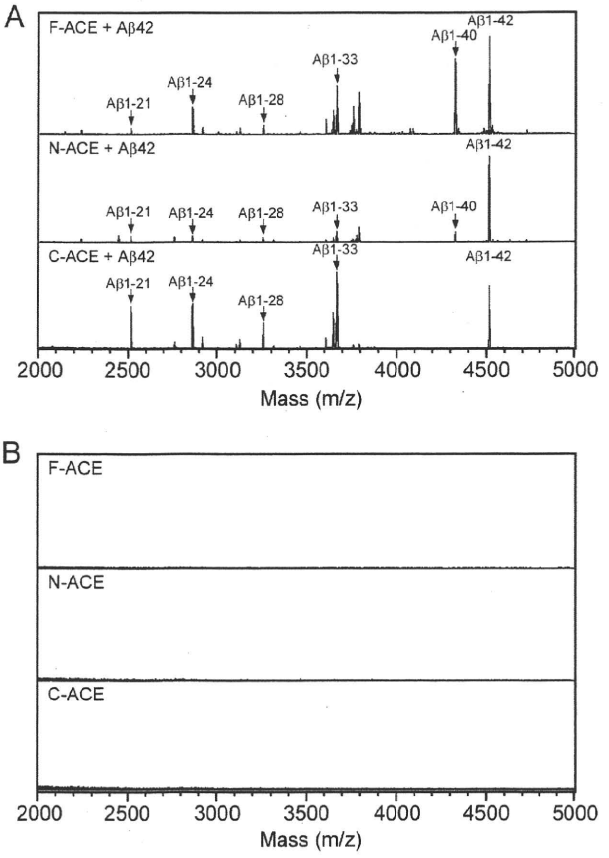

FIGURE 2. **MALDI-TOF-MS analysis for Aβ42 degradation by F-ACE, N-ACE, or C-ACE.** *A*, Aβ42 (80 μM) was incubated with 0.5 μM purified F-ACE, N-ACE, or C-ACE at 37 °C for 2 h, then captopril (10 μM) was added after incubation to stop the digestion. 1 μl of the mixture was subjected to MALDI-TOF-MS analysis. F-ACE and N-ACE generated Aβ1–40, whereas C-ACE did not. *B*, 1 μl of F-ACE, N-ACE, or C-ACE alone incubated at 37 °C for 2 h was subjected to MALDI-TOF-MS analysis, and a peptide signal was not detected.

wtACE, whereas E362D and E362/960D without N-domain activity did not convert Aβ42 to Aβ40 (Fig. 3*D*, *middle panel*).

N-Glycosylation Is Essential for Aβ42-to-Aβ40- and Angiotensin-converting Activities—ACE is a glycoprotein, and the *N*-linked glycosylation of testicular ACE has been shown to be essential for its angiotensin-converting activity. Human ACE has 17 putative Asn*X*(Ser/Thr) *N*-linked glycosylation sites distributed throughout both the N-domain and C-domain (21). To determine the role of glycosylation of ACE in its enzymatic activities and to compare the glycosylation of natural human ACE with that of recombinant F-ACE, N-ACE, and C-ACE, we examined the type of glycosylation of these ACE proteins by the treatment with PNGase F, *O*-glycanase, and sialidase A. Treatment with PNGase F, *O*-glycanase, and sialidase A remarkably reduced the molecular weight of human kidney ACE, F-ACE, N-ACE, and C-ACE (Fig. 4*A*, *lanes 1* and *2*). Removal of *N*-linked glycosylation using PNGase F alone produced similar molecular weight shifts, whereas *O*-glycanase did not produce any shift in ACE size (Fig. 4*A*, *lanes 3* and *4*). The sensitivity of N-ACE to PNGase F indicates that N-ACE is modified by *N*-linked glycosylation. All the ACE proteins showed a slight decrease in the molecular weight after sialidase A digestion,

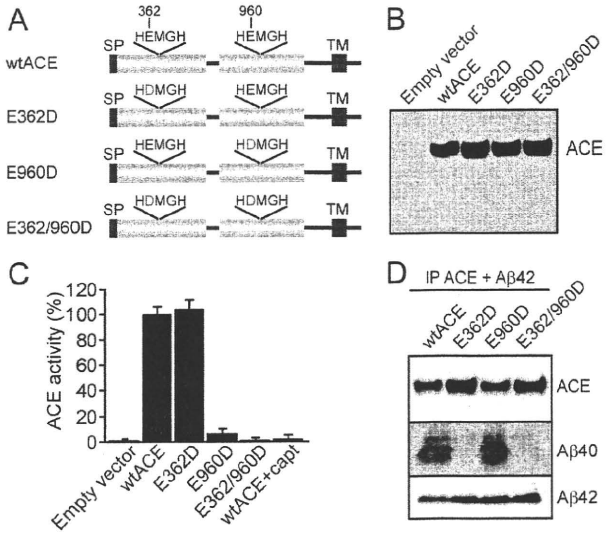

FIGURE 3. **Site-directed mutated ACE proteins exhibit domain-specific Aβ42-to-Aβ40- and angiotensin-converting activity.** *A*, schematic representation of human ACE and the mutant positions. The two ACE zinc metalloprotease active site glutamates (amino acids 362 in the N-domain and 960 in the C-domain) were changed to aspartates. *B*, fibroblasts were transiently transfected with empty vector, wtACE or mutant ACE plasmids and the expression of ACE proteins was detected by Western blotting using a polyclonal anti-ACE antibody. *C*, ACE activity was measured by incubating 5 μg of protein of cell lysate with the substrate Hip-His-Leu for 10 min at 37 °C. ACE activity in cell lysate was clearly detected in wtACE and E362D. C-domain inactive ACE protein, E960D, showed an extremely low ACE activity; and double mutants in both domains of ACE, E362/960D, did not show ACE activity. ACE activity was clearly inhibited by captopril (1 μM) treatment. *D*, ACE in cell lysate (4 mg of protein) from each transfected cell line was immunoprecipitated by 5 μg of polyclonal anti-ACE antibody and 100 μl of protein G-Sepharose. Immunoprecipitated ACE was then incubated with synthetic Aβ42 and the generation of Aβ40 was detected by Western blotting. *SP*, signal peptide; *TM*, transmembrane.

indicating the sialylation of their *N*-glycans (Fig. 4*A*, *lane 5*). These results suggest that the glycosylation type of natural human kidney ACE and recombinant ACE proteins produced by COS7 cells are identical. Because ACE is modified by *N*-linked glycosylation and *O*-linked glycosylation was not detected, we used PNGase to remove its *N*-glycans and studied the ACE activity. As expected, PNGase-treated human kidney ACE showed a 96% reduced ACE activity in degradation of Hip-His-Leu compared with untreated ACE (Fig. 4*B*).

To determine the role of *N*-linked glycosylation of ACE in its Aβ42-to-Aβ40-converting activity, we incubated Aβ42 with PNGase F-treated or untreated human kidney ACE and examined Aβ40 generation by Western blot. Deglycosylated human kidney ACE showed a decreased molecular mass at ~150 kDa and was degraded by itself after 2 h of incubation. After incubation for 16 h, ~150-kDa deglycosylated ACE was completely degraded (Fig. 4*C*, *upper panel*). Aβ40 was generated from Aβ42 by ACE after incubating the mixture of Aβ42 and ACE for 15 min. The level of Aβ40 increased in a time-dependent manner and reached a peak after incubation for 2 h, whereas deglycosylated ACE did not generate Aβ40 from Aβ42, although it showed a similar Aβ42-degrading activity compared with non-deglycosylated ACE (Fig. 4*C*, *middle and bottom panels*). This glycosylation-required Aβ42-to-Aβ40-converting activity was also confirmed in recombinant ACE proteins. PNGase F-deglycosylated F-ACE, N-ACE, and C-ACE have similar Aβ42-degrading activity. However, deglycosylated F-ACE and N-ACE failed to generate Aβ40 from Aβ42, suggesting that the *N*-linked glycosylation in the ACE N-domain is essential for its Aβ42-to-Aβ40-converting activity (Fig. 4*D*). Sialidase A treatment did not change the Aβ42-to-Aβ40-converting activity and the ACE activity of human kidney ACE, indicating that sialylation is not required for its activities (data not shown).

Captopril and Enalaprilat Showed Different IC_{50} on Aβ42-to-Aβ40-converting Activity—The feature of ACE inhibitors has been well studied in terms of their angiotensin-converting inhibitory effect. To explore whether ACE inhibitors differentially inhibit the Aβ42-to-Aβ40-converting activity, we determined the IC_{50} of captopril, perindopril, lisinopril, and enalaprilat toward the angiotensin- and Aβ42-to-Aβ40-converting activity of F-ACE. All four ACE inhibitors showed a similar IC_{50} on the inhibition of angiotensin-converting activity of F-ACE, whereas enalaprilat exhibited a 10-fold lower IC_{50} (0.003~0.01 μM) on Aβ42-to-Aβ40-converting activity than captopril (0.03~0.1 μM) (Table 1).

DISCUSSION

Most mammalian tissues contain ACE with two catalytic domains. Evolutionary conservation of the ACE N- and C-domains suggests important distinct functions of these domains. Recent genetic studies have associated the I allele of the *ACE* gene, which results in a reduced serum ACE level, with onset of AD (1, 3). We have shown previously that ACE converts Aβ42 to Aβ40, and its inhibition predominantly enhances brain Aβ42 deposition (15). To investigate which domain of ACE is responsible for Aβ42-to-Aβ40-converting activity and whether ACE inhibitors inhibit this activity, we generated three kinds of ACE proteins, containing both N- and C-domains or containing either single active domain. We also used selective site-directed mutagenesis of ACE to study the domain-specific activity of full-length ACE. The present study shows that the Aβ42-to-Aβ40- and angiotensin-converting activities were located in different ACE domains and that *N*-linked glycosylation was essential for the two ACE enzymatic activities. The N-domain of ACE clearly showed an Aβ42-to-Aβ40-converting activity, whereas it has an extremely low angiotensin-converting activity. In contrast, the C-domain of ACE showed angiotensin-converting activity, whereas the Aβ42-to-Aβ40-converting activity was not detected in this domain.

In a cellular context, both the N-domain and C-domains of ACE are able to degrade Aβ40 and Aβ42 (9). In our studies, we also found that the N- and C-domains were indistinguishable as regarding degrading Aβ42, suggesting that both N- and C-domains of ACE have endopeptidase activity for Aβ42. In the overall scheme of Aβ42 processing, the full-length ACE cleaving into many fragments may be important for therapeutic treatment of AD. We showed that Aβ40, but not Aβ41, was generated from Aβ42 (Fig. 2*A*). However, the Aβ42-to-Aβ40-converting activity was solely found in the N-domain of ACE (Figs. 1, 2, and 3). These results suggest that the dipeptidyl carboxypeptidase activity converting Aβ42 to Aβ40 is restricted to its N-domain. The N-domain specific dipeptidyl activity was

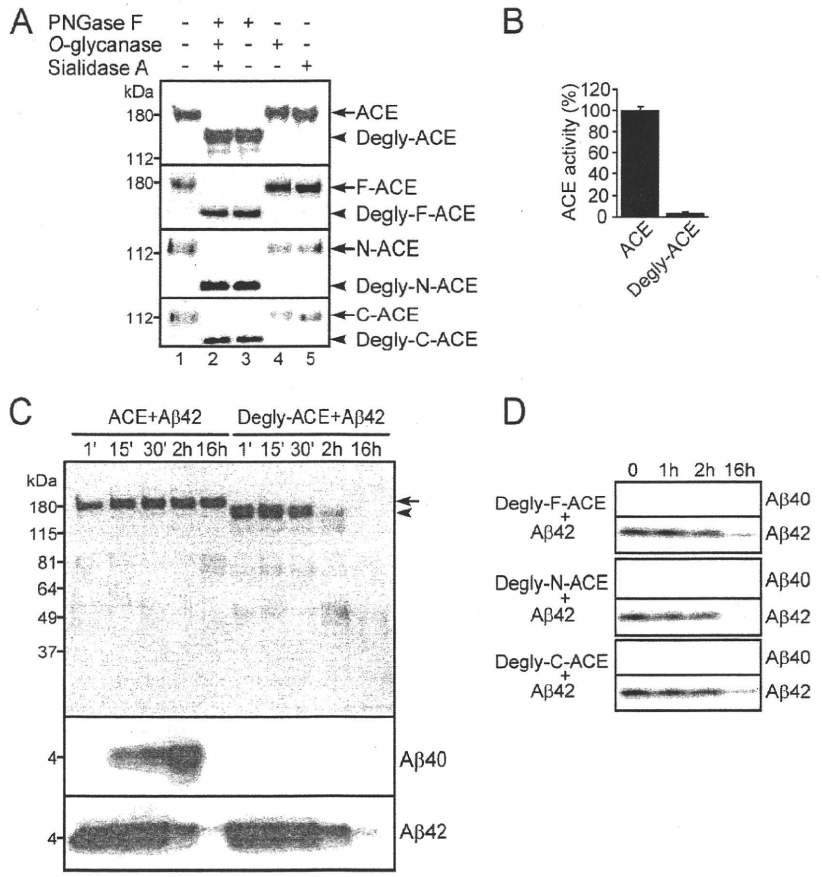

FIGURE 4. **Characterization of ACE glycosylation and role of the glycosylation in ACE activity and Aβ42-to-Aβ40-converting activity.** *A*, 5 μg of purified human kidney ACE, F-ACE, N-ACE, and C-ACE were deglycosylated with 1 μl of PNGase F, *O*-glycanase, and/or sialidase A for 1 h at 37 °C. PNGase F alone was able to remove all glycosylation of ACE. *B*, ACE activity of PNGase F-deglycosylated human kidney ACE was measured immediately after deglycosylation using an ACE colorimetric kit. ACE activity was almost completely abolished by *N*-deglycosylation. *C*, 80 μl of human kidney ACE (0.5 μM) with or without *N*-deglycosylation was mixed with synthetic Aβ42 (40 μM) and incubated at 37 °C. 10 μl of the mixture were collected at various incubation time points and subjected to Western blot analysis. Deglycosylated ACE showed no Aβ42-to-Aβ40-converting activity, whereas the Aβ42-degrading activity remained. *D*, 40 μl of recombinant F-, N-, and C-ACE proteins (0.5 μM) were deglycosylated and mixed with Aβ42 and incubated at 37 °C for 1, 2, or 16 h. Aβ42-to-Aβ40-converting activity was not detected in either deglycosylated F-ACE or deglycosylated N-ACE, whereas all the deglycosylated ACE showed an Aβ42-degrading activity.

and angiotensin-converting activity, respectively, compared with full domain ACE (Fig. 1, *C* and *F*), suggesting that each catalytic domain of ACE regulates the activity of the other, and both domains are required for normal substrate recognition and degradation. Mice with a selective inactivation of either the N- or C-domain of ACE were generated, and the C-domain was demonstrated to be the main site of angiotensin I cleavage (18, 22), which is consistent with our *in vitro* finding. However, the role of the N-domain of ACE toward Aβ42 to Aβ40 conversion *in vivo* needs to be addressed.

It has been previously reported that testicular ACE, the C-domain isoform of ACE, without *N*-linked glycosylation has no enzyme activity and was rapidly degraded (19). We confirmed that deglycosylation of human kidney ACE abolished its angiotensin-converting activity, whereas the endopeptidase activity for degrading itself and Aβ42 was not affected. Moreover, the N-domain-specific Aβ42-to-Aβ40-converting activity was abolished by the deglycosylation, indicating that the *N*-linked glycosylation is also essential for maintaining the N-domain-specific enzymatic activity of ACE. Deglycosylated ACE was retained as an intact protein 30 min after deglycosylation. ACE activity and Aβ42-to-Aβ40-converting activity were clearly detected in non-deglycosylated ACE within 30 min (Fig. 4, *B* and *C*). Thus, the loss of ACE activity and Aβ42-to-Aβ40-converting activity of deglycosylated ACE may not result from its self-degradation, but likely result from the deglycosylation. These results suggest that *N*-linked glycosylation is required to maintain the ACE structure and its dipeptidyl carboxypeptidase activity in both N- and C-domains. Presenilins have been shown to be involved in the maturation of membrane proteins, whether presenilin mutants in familial AD affect ACE glycosylation and its Aβ42-to-Aβ40-converting activity need to be clarified in future (23). Finally, we showed that ACE inhibitors inhibited the N-domain-specific Aβ42-to-Aβ40-converting activity each with a different IC_{50}. Among the examined ACE inhibitors, enalaprilat has the strongest inhibitory effect on Aβ42-to-Aβ40-converting activity. This result may provide a mechanism underlying the finding that non-centrally active ACE inhibitors, such as enalapril, are associated with a greater risk of incident dementia (24). In

TABLE 1

ACE inhibitors inhibited Aβ42-to-Aβ40-converting activity with different IC_{50}

ACE activity of 10 μl of F-ACE (0.5 μM) was measured using an ACE colorimetric kit, and Aβ42-to-Aβ40-converting activity was measured by Western blotting and densitometry. 0, 0.003, 0.01, 0.03, 0.1, 0.3, 1, 3, 10 μM ACE inhibitors were added to determine the IC_{50} for Aβ42-to-Aβ40-converting activity.

ACE inhibitors	ACE activity IC_{50}	Aβ-converting activity IC_{50}[a]
	μM	μM
Captopril	0.01–0.03	0.03–0.1
Enalaprilat	0.01–0.03	0.003–0.01
Lisinopril	0.01–0.03	0.01–0.03
Perindopril	0.03–0.1	0.01–0.03

[a] Aβ-converting activity, Aβ42-to-Aβ40-converting activity.

also found in the degradation of AcSDKP, which is involved in the control of hematopoietic stem cell proliferation. The molecular basis in which the N-domain of ACE accesses AcSDKP and Aβ42 remains to be elucidated. The N- and C-domains of ACE have reduced Aβ42-to-Aβ40-converting activity

our previous *in vivo* study, captopril treatment enhanced predominantly brain Aβ42 deposition in 17-month-old amyloid precursor protein (APP) transgenic mice and led to a tendency of increased brain Aβ42/40 ratio (15). Taking the anti-amyloid and antioxidant effects of Aβ40 into account, our findings suggest that ACE inhibitors could be designed specifically to target the C-domain of ACE without inhibiting its N-domain-specific Aβ42-to-Aβ40-converting activity.

Acknowledgments—We thank Dr. Dennis J. Selkoe for providing wtACE, E362D, E960D, and E362/960D plasmids and thank Dr. Paul Langman for English correction.

REFERENCES

1. Kehoe, P. G., and Wilcock, G. K. (2007) *Lancet Neurol.* **6,** 373–378
2. Zou, K., and Michikawa, M. (2008) *Rev. Neurosci.* **19,** 203–212
3. Lehmann, D. J., Cortina-Borja, M., Warden, D. R., Smith, A. D., Sleegers, K., Prince, J. A., van Duijn, C. M., and Kehoe, P. G. (2005) *Am. J. Epidemiol.* **162,** 305–317
4. Kehoe, P. G., Russ, C., McIlory, S., Williams, H., Holmans, P., Holmes, C., Liolitsa, D., Vahidassr, D., Powell, J., McGleenon, B., Liddell, M., Plomin, R., Dynan, K., Williams, N., Neal, J., Cairns, N. J., Wilcock, G., Passmore, P., Lovestone, S., Williams, J., and Owen, M. J. (1999) *Nat. Genet.* **21,** 71–72
5. Elkins, J. S., Douglas, V. C., and Johnston, S. C. (2004) *Neurology* **62,** 363–368
6. Skoog, I., Lernfelt, B., Landahl, S., Palmertz, B., Andreasson, L. A., Nilsson, L., Persson, G., Odén, A., and Svanborg, A. (1996) *Lancet* **347,** 1141–1145
7. Khachaturian, A. S., Zandi, P. P., Lyketsos, C. G., Hayden, K. M., Skoog, I., Norton, M. C., Tschanz, J. T., Mayer, L. S., Welsh-Bohmer, K. A., and Breitner, J. C. (2006) *Arch. Neurol.* **63,** 686–692
8. Hu, J., Igarashi, A., Kamata, M., and Nakagawa, H. (2001) *J. Biol. Chem.* **276,** 47863–47868
9. Hemming, M. L., and Selkoe, D. J. (2005) *J. Biol. Chem.* **280,** 37644–37650
10. Mucke, L., Masliah, E., Yu, G. Q., Mallory, M., Rockenstein, E. M., Tatsuno, G., Hu, K., Kholodenko, D., Johnson-Wood, K., and McConlogue, L. (2000) *J. Neurosci.* **20,** 4050–4058
11. McGowan, E., Pickford, F., Kim, J., Onstead, L., Eriksen, J., Yu, C., Skipper, L., Murphy, M. P., Beard, J., Das, P., Jansen, K., Delucia, M., Lin, W. L., Dolios, G., Wang, R., Eckman, C. B., Dickson, D. W., Hutton, M., Hardy, J., and Golde, T. (2005) *Neuron* **47,** 191–199
12. Zou, K., Gong, J. S., Yanagisawa, K., and Michikawa, M. (2002) *J. Neurosci.* **22,** 4833–4841
13. Zou, K., Kim, D., Kakio, A., Byun, K., Gong, J. S., Kim, J., Kim, M., Sawamura, N., Nishimoto, S., Matsuzaki, K., Lee, B., Yanagisawa, K., and Michikawa, M. (2003) *J. Neurochem.* **87,** 609–619
14. Kim, J., Onstead, L., Randle, S., Price, R., Smithson, L., Zwizinski, C., Dickson, D. W., Golde, T., and McGowan, E. (2007) *J. Neurosci.* **27,** 627–633
15. Zou, K., Yamaguchi, H., Akatsu, H., Sakamoto, T., Ko, M., Mizoguchi, K., Gong, J. S., Yu, W., Yamamoto, T., Kosaka, K., Yanagisawa, K., and Michikawa, M. (2007) *J. Neurosci.* **27,** 8628–8635
16. Turner, A. J., and Hooper, N. M. (2002) *Trends Pharmacol. Sci.* **23,** 177–183
17. Rousseau, A., Michaud, A., Chauvet, M. T., Lenfant, M., and Corvol, P. (1995) *J. Biol. Chem.* **270,** 3656–3661
18. Fuchs, S., Xiao, H. D., Hubert, C., Michaud, A., Campbell, D. J., Adams, J. W., Capecchi, M. R., Corvol, P., and Bernstein, K. E. (2008) *Hypertension* **51,** 267–274
19. Sadhukhan, R., and Sen, I. (1996) *J. Biol. Chem.* **271,** 6429–6434
20. Oba, R., Igarashi, A., Kamata, M., Nagata, K., Takano, S., and Nakagawa, H. (2005) *Eur. J. Neurosci.* **21,** 733–740
21. Soubrier, F., Alhenc-Gelas, F., Hubert, C., Allegrini, J., John, M., Tregear, G., and Corvol, P. (1988) *Proc. Natl. Acad. Sci. U.S.A.* **85,** 9386–9390
22. Fuchs, S., Xiao, H. D., Cole, J. M., Adams, J. W., Frenzel, K., Michaud, A., Zhao, H., Keshelava, G., Capecchi, M. R., Corvol, P., and Bernstein, K. E. (2004) *J. Biol. Chem.* **279,** 15946–15953
23. Zou, K., Hosono, T., Nakamura, T., Shiraishi, H., Maeda, T., Komano, H., Yanagisawa, K., and Michikawa, M. (2008) *Biochemistry* **47,** 3370–3378
24. Sink, K. M., Leng, X., Williamson, J., Kritchevsky, S. B., Yaffe, K., Kuller, L., Yasar, S., Atkinson, H., Robbins, M., Psaty, B., and Goff, D. C., Jr. (2009) *Arch. Intern. Med.* **169,** 1195–1202

Brain Pathology ISSN 1015-6305

RESEARCH ARTICLE

Transthyretin Accelerates Vascular Aβ Deposition in a Mouse Model of Alzheimer's Disease

Henny Wati[1]; Takeshi Kawarabayashi[2]; Etsuro Matsubara[3]; Ayumi Kasai[4]; Takae Hirasawa[5]; Takeo Kubota[5]; Yasuo Harigaya[6]; Mikio Shoji[2]; Shuichiro Maeda[1]

[1] Department of Biochemistry, Interdisciplinary Graduate School of Medicine and Engineering, University of Yamanashi, 1110 Shimokato, Chuo, Yamanashi 409-3898, Japan.
[2] Department of Neurology, Hirosaki University School of Medicine, 5 Zaifu, Hirosaki 036-8562, Japan.
[3] Department of Alzheimer's Disease Research, National Institute for Longevity Sciences, National Center for Geriatrics and Gerontology, 36-3 Gengo, Morioka, Obu, Aichi 474-8522, Japan.
[4] Department of Molecular Signaling, Interdisciplinary Graduate School of Medicine and Engineering, University of Yamanashi, 1110 Shimokato, Chuo, Yamanashi 409-3898, Japan.
[5] Department of Epigenetic Medicine, Interdisciplinary Graduate School of Medicine and Engineering, University of Yamanashi, 1110 Shimokato, Chuo, Yamanashi 409-3898, Japan.
[6] Neurology Service, Maebashi Red Cross Hospital, 3-21-36 Asahi, Maebashi, Tokyo 371-0014, Japan.

Keywords
Alzheimer's disease, amyloid-β, apoptosis, tau phosphorylation, Tg2576 mouse, Transthyretin.

Corresponding author:
Shuichiro Maeda, Department of Biochemistry, Interdisciplinary Graduate School of Medicine and Engineering, University of Yamanashi, 1110 Shimokato, Chuo, Yamanashi 409-3898, Japan (Email: *smaeda@yamanashi.ac.jp*)

Received 12 October 2007; revised: 10 February 2008; accepted 12 February 2008.

doi:10.1111/j.1750-3639.2008.00166.x

Abstract

Transthyretin (TTR) binds amyloid-β (Aβ) and prevents Aβ fibril formation *in vitro*. It was reported that the lack of neurodegeneration in a transgenic mouse model of Alzheimer's disease (AD) (Tg2576 mouse) was associated with increased TTR level in the hippocampus, and that chronic infusion of anti-TTR antibody into the hippocampus of Tg2576 mice led to increased local Aβ deposits, tau hyperphosphorylation and apoptosis. TTR is, therefore, speculated to prevent Aβ pathology in AD. However, a role for TTR in Aβ deposition is not yet known. To investigate the relationship between TTR and Aβ deposition, we generated a mouse line carrying a null mutation at the endogenous *TTR* locus and the human mutant amyloid precursor protein cDNA responsible for familial AD (Tg2576/$TTR^{-/-}$ mouse) by crossing Tg2576 mice with TTR-deficient mice. We asked whether Aβ deposition was accelerated in Tg2576/$TTR^{-/-}$ mice relative to the heterozygous mutant Tg2576 (Tg2576/$TTR^{+/-}$) mice. Contrary to our expectations, the degree of total and vascular Aβ burdens in the aged Tg2576/$TTR^{-/-}$ mice was significantly reduced relative to the age-matched Tg2576/$TTR^{+/-}$ mice. Our experiments present, for the first time, compelling evidence that TTR does not suppress but rather accelerates vascular Aβ deposition in the mouse model of AD.

INTRODUCTION

Insoluble amyloid-β (Aβ) peptides, the main components of brain amyloid plaques, are thought to be the causative agent of Alzheimer's disease (AD) (11). However, Aβ is normally present in a soluble form in plasma and in the cerebrospinal fluid (CSF) (39, 40), suggesting that some other factors may modulate the aggregation of Aβ fibrils. The hypothesis that transthyretin (TTR) might play some role in the pathogenesis of AD originated from the observation that TTR in the CSF binds Aβ, and prevents Aβ fibril formation *in vitro* (36, 37). It was further observed that the levels of both TTR and its oxidized forms in the CSF were lower in patients with AD compared with the age-matched controls (2, 38). The importance of TTR in inhibition of Aβ fibril formation and toxicity *in vivo* was also suggested in two model systems: transgenic *Caenorhabditis elegans* and a transgenic mouse model of AD, Tg2576. Link reported that co-expression of Aβ peptide and TTR in transgenic *C. elegans* led to a reduction in Aβ deposits (22). Tg2576 line has high level of plasma Aβ peptides (14, 18), and develops brain Aβ deposits similar to that seen in patients with AD (15, 35) and behavioral deficits (13, 53). However, it lacks neurofibrillary tangles (NFT) (27, 48, 49) and neuronal loss (15), which are unique characteristics of patients with AD (5). Stein and Johnson reported that the lack of neurodegeneration was associated with increased level of TTR in the hippocampus of Tg2576 (43). They also reported that chronic infusion of an antibody against TTR into the hippocampus of Tg2576 mice led to increased Aβ deposits, tau hyperphosphorylation, neuronal loss and apoptosis in the CA1 neuronal field (42). Carro *et al* reported that reduced Aβ burden after insulin-like growth factor I-treatment of Tg2576 was paralleled by increased brain levels of TTR (6). Giunta *et al* reported the inhibition of Aβ aggregation and toxicity and Aβ-induced apoptotic changes by TTR in cultured cells (10).

All these findings support for the importance of TTR in prevention of Aβ aggregation and toxicity. However, a role for TTR in Aβ deposition is not yet known. To investigate the relationship between TTR and Aβ deposition, we generated a mouse line carrying a null mutation at the endogenous *TTR* locus and the human mutant amyloid precursor protein (APP) cDNA responsible for familial AD (Tg2576/$TTR^{-/-}$ mouse), by crossing Tg2576 mice with TTR-deficient mice generated through gene targeting (9). We asked whether Aβ deposition was accelerated in Tg2576/$TTR^{-/-}$ mice relative to the heterozygous mutant Tg2576 (Tg2576/$TTR^{+/-}$) mice.

METHODS

Animals

Transgenic mice producing human variant APP and lacking endogenous mouse TTR were generated as follows. A male Tg2576 mouse (13) carrying the human mutant APP cDNA with the double mutation K670N and M671L responsible for Swedish familial AD backcrossed to C57BL/6 for 2 generations was mated with $TTR^{-/-}$ female mice backcrossed to C57BL/6 for eight generations (9). The $TTR^{+/-}$ F1 male mice carrying the mutant APP cDNA were mated with $TTR^{-/-}$ female mice. Heterozygous ($TTR^{+/-}$) F2 male mice carrying the mutant APP cDNA (Tg2576/$TTR^{+/-}$) were mated with $TTR^{-/-}$ F2 female mice. The $TTR^{+/-}$ and $TTR^{-/-}$ F3 progenies carrying the mutant APP cDNA (Tg2576/$TTR^{+/-}$ and Tg2576/$TTR^{-/-}$) were used in the present study. The F3 transgenic mice were maintained in cages housing three to six mice each, on separate racks in the same room, kept under a 12-h light cycle. Regular rodent's chow (Oriental Yeast, Tokyo, Japan) and tap water were freely available.

Transgenic mice were killed by cervical dislocation after anesthesia with diethyl ether. The brains were dissected; the right hemi-brains were immediately frozen in liquid nitrogen and stored at −80°C while the left hemi-brains were fixed in 4% buffered paraformaldehyde, and embedded in paraffin. Genotype analysis for each animal was carried out by polymerase chain reaction on DNA, purified from tails, as described (9, 14). The presence and absence of TTR in the serum of Tg2576/$TTR^{+/-}$, and Tg2576/$TTR^{-/-}$ mice, respectively, were confirmed by western blotting analysis as described (51).

All animal experiments were approved by University of Yamanashi Animal Care and Use Committee.

Immunohistochemistry

For brain Aβ detection, the paraffin-embedded left hemi-brain sections (5 μm) were pretreated with 99% formic acid for 3 minutes and immersed in 5% periodic acid for 10 minutes to block endogenous peroxidase. They were then incubated with blocking buffer [5% normal goat serum (Gibco, Carlsbad, CA, USA) in 10-mM phosphate buffer pH 7.4 and 100-mM NaCl with 0.05% Tween-20 (Bio-Rad, Richmond, CA, USA) containing Block Ace (Dainipponseiyaku, Suita, Japan)] for 1 h, with primary antibody [Ab9204 recognizing normal L-aspartate at position 1 (34), 0.1 μg/ml] overnight, and with biotinylated anti-rabbit immunoglobulin G (IgG) antibody (1:200) (Vector Laboratories, Burlingame, CA, USA) for 1 h. Immunoreactivity was visualized with the use of Vectastain ABC Elite kit (Vector Laboratories, Burlingame, CA, USA), and 3,3′-diaminobenzidine, tetrahydrocloride (DAB). Tissue sections were counterstained with hematoxylin.

For phosphorylated tau detection, the paraffin sections were pretreated with periodic acid, as described above and then irradiated in 10-mM citric acid buffer pH 6.0 for 15 minutes with microwave oven. After blocking, as described above, the sections were stained with the use of primary antibody AT8, recognizing phosphorylated tau at Ser202/Thr205 (1:500) (Innogenetics, Gent, Belgium) or anti-phosphorylated tau, recognizing phosphorylated tau at Thr231 (Thr231; 1:1000) (Calbiochem, Darmstadt, Germany), and Vectastain ABC Elite kit and counterstained by hematoxylin.

Fragmented DNA of apoptotic cells in the brain was detected by terminal deoxynucleotidyl transferase-mediated dUTP nick end labeling (TUNEL) method with the use of DeadEnd Colorimetric TUNEL System (Promega, Madison, WI, USA) and DAB according to the manufacturer's instructions.

Quantification of Aβ burden by image analysis

For quantification of Aβ burden, immuno-labeling was examined in the entire cerebral cortex and hippocampal areas of Tg2576/$TTR^{+/-}$ and Tg2576/$TTR^{-/-}$ mice. The amyloid burden was calculated by dividing total area of Aβ deposits by total area of region analyzed (in pixels). Images were captured and analyzed with the use of ImagePro®ver6 software (Media Cybernetics, Silver Spring, MD, USA). Four coronal sections from each of the mice were examined. The burden was expressed as mean ± standard error of the mean.

Protein extraction

Frozen right hemi-brains were sequentially extracted using two-step extraction method, as described previously (18). Initially, the frozen brain samples were homogenized in 2% sodium dodecylsulfate (SDS) (150 mg/ml wet weight) with protease inhibitors (complete protease inhibitor cocktail, one tablet in 50-ml solution; Boehringer Mannheim, Mannheim, Germany) followed by centrifugation at 100,000 *g* for 1 h at 4°C. The supernatant was then removed (termed SDS fraction), and the resultant pellet was sonicated [(35 s at level 10; XL-2000 Microson Ultrasonic Cell Disruptor (Misonix Inc., Farmingdale, NY, USA)] in 70% formic acid in water. After sonication, the samples were centrifuged, as described above, and the supernatant was removed (termed FA fraction). Total protein concentration measurement for SDS fraction was carried out with the use of BCA Kit (Pierce, Rockford, IL, USA).

Western blotting analysis

The SDS fractions of brain extracts (30 μg of protein) were electrophoresed on 4–12% gradient Bis-Tris gels (NuPage, Invitrogen, Carlsbad, CA, USA) and transferred to polyvinylidene difluoride membranes (Tefco, Tokyo, Japan). Membranes were labeled with the use of primary antibody, Saeko (1:1000), recognizing C terminal 30 amino acids of both human and mouse APP (18) overnight at 4°C, incubated with horseradish peroxidase-linked anti-rabbit IgG antibody (Amersham Biosciences, Buckingham, UK) (1:2000) for 1 h, and the immunoreactivity was visualized with the use of Supersignal (Pierce, Rockford, IL, USA). Images were captured by Fuji Bas-1000 imaging analyzer (Fujifilm, Tokyo, Japan), and the

intensity of the bands was quantified with the use of Scion Image (Scion Corp., Frederick, MD, USA).

Sandwich enzyme-linked immunosorbent assay

Amyloid-β 40 and Aβ42 in the brain extracts (SDS and FA fractions) were measured by sandwich enzyme-linked immunosorbent assay (ELISA), as described previously (18, 24, 25). Microplates (Immunoplate I, Nunc, Rockilde, Denmark) were pre-coated with anti-Aβ monoclonal antibody BNT77 (IgA isotype specific for Aβ11-16) that recognizes both Aβ40 and Aβ42, then incubated for 24 h at 4°C with 100 μl/well of samples. The microplates were further incubated for 24 h at 4°C with either horseradish-peroxidase-conjugated BA27 (anti-Aβ1-40, specific for Aβ40) or BC-05 (anti-Aβ35-43, specific for Aβ42 and Aβ43). Color was developed with 3,3′,5,5′-tetramethylbenzidine and evaluated at 450 nm on a microplate Reader (Molecular Devices, Menlo Park, CA, USA). The SDS fractions were diluted 400 times in EC buffer [20-mM phosphate buffer, pH 7.0, 400-mM NaCl, 2-mM EDTA, 0.4% Block Ace (Dainipponseiyaku, Suita, Japan), 0.2% bovine serum albumin, 0.05% CHAPS and 0.05% sodium azide] containing 0.005% SDS. The FA fraction was neutralized by a 1:50 dilution into 1-M Tris-HCl, pH 8.0 and then further diluted 20 times in EC buffer. The program Softmax (Molecular Devices, Menlo Park, CA, USA) was used to calculate Aβ concentration (in picomolar) by comparing the sample absorbance with the absorbance of known concentrations of synthetic Aβ42 or Aβ40 standards (Sigma, St Louis, MO, USA) assayed identically on the same plate. Using the wet weight of brain in the original homogenate, the final values of Aβ in brain were expressed as picomoles per gram wet weight.

Statistical analysis

The difference in the Aβ burden between Tg2576/*TTR*$^{+/-}$ and Tg2576/*TTR*$^{-/-}$ mice was examined with ANOVA followed by the Student's unpaired *t*-test with GraphPad Prism, Version 4.0 (GraphPad Software, San Diego, CA, USA). $P < 0.05$ was considered significant.

RESULTS

There is no significant difference in the brain levels of full-length APP between Tg2576/TTR$^{+/-}$ and Tg2576/TTR$^{-/-}$ mice

Amyloid-β peptides are derived from APP. To determine whether or not TTR affected the level of full-length APP, the groups of two Tg2576/*TTR*$^{+/-}$ and Tg2576/*TTR*$^{-/-}$ littermates were killed at 16, 18 and 20 months of age, and relative levels of full-length APP in the SDS fractions prepared from the brain were determined by western blotting with the use of Saeko, as described under *Methods*. Significant differences were never detected in the levels of full-length APP among any of the Tg2576/*TTR*$^{+/-}$ and Tg2576/*TTR*$^{-/-}$ mice examined (Figure 1). Thus, TTR does not affect the level of full-length APP in the brain of Tg2576 mice.

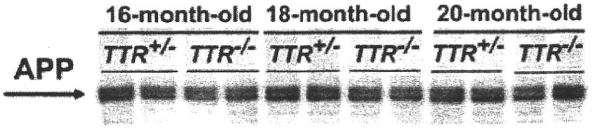

Figure 1. *Western blotting analysis of full-length amyloid precursor protein (APP).* The arrow on the left indicates the location of full-length APP.

Transthyretin deficiency does not increase but decreases the degree of total and vascular Aβ burdens in the brain of Tg2576 mice

Total Aβ burden

To evaluate whether or not TTR affected Aβ deposition, we compared the onset, progression and distribution of amyloid deposition between the brain of Tg2576/*TTR*$^{+/-}$ and Tg2576/*TTR*$^{-/-}$ mice, measuring the area occupied by Aβ deposits around the vascular wall of the meninx and cerebral parenchyma (termed cerebral amyloid angiopathy; CAA) and inside the brain parenchyma (termed Aβ plaque), as described under *Methods*. A time-course analysis of the total Aβ deposition in the brain was performed by assessing mice of ages 7–20 months. The number and age of mice examined were shown in Table 1. Aβ deposits were not detected in any of the six 7–11-month-old Tg2576/*TTR*$^{+/-}$ and Tg2576/*TTR*$^{-/-}$ mice examined. A small amount of Aβ deposits was first observed at 12 months of age in both the mice (data not shown). With advancing age, total Aβ burden increased (Figure 2A), and Aβ deposits were observed in the cerebral cortex, neocortex and hippocampus (Figure 3A), but not in the cerebellum (data not shown) in both the mice. Although there was a trend to reduction of total Aβ burden in 12–17-month-old Tg2576/*TTR*$^{-/-}$ mice relative to the age-matched Tg2576/*TTR*$^{+/-}$ mice, there was no statistically significant difference in the onset, progression and distribution of total Aβ deposition in the entire cerebral cortex between Tg2576/*TTR*$^{+/-}$ and Tg2576/*TTR*$^{-/-}$ mice (Figure 2A). The size of Aβ deposits in Tg2576/*TTR*$^{-/-}$ mice was also much the same as that in the age-matched Tg2576/*TTR*$^{+/-}$ mice. In 18–20-month-old Tg2576/*TTR*$^{-/-}$

Table 1. The number and age of mice examined by immunohistochemistry. Abbreviation: n = number of mice.

Age (months)	Tg2576/*TTR*$^{+/-}$ (n)	Tg2576/*TTR*$^{-/-}$ (n)
7	2	2
8	2	2
11	2	2
12	2	2
13	5	5
14	6	6
15	6	6
16	6	6
17	3	3
18	6	6
20	2	2
Total	42	42

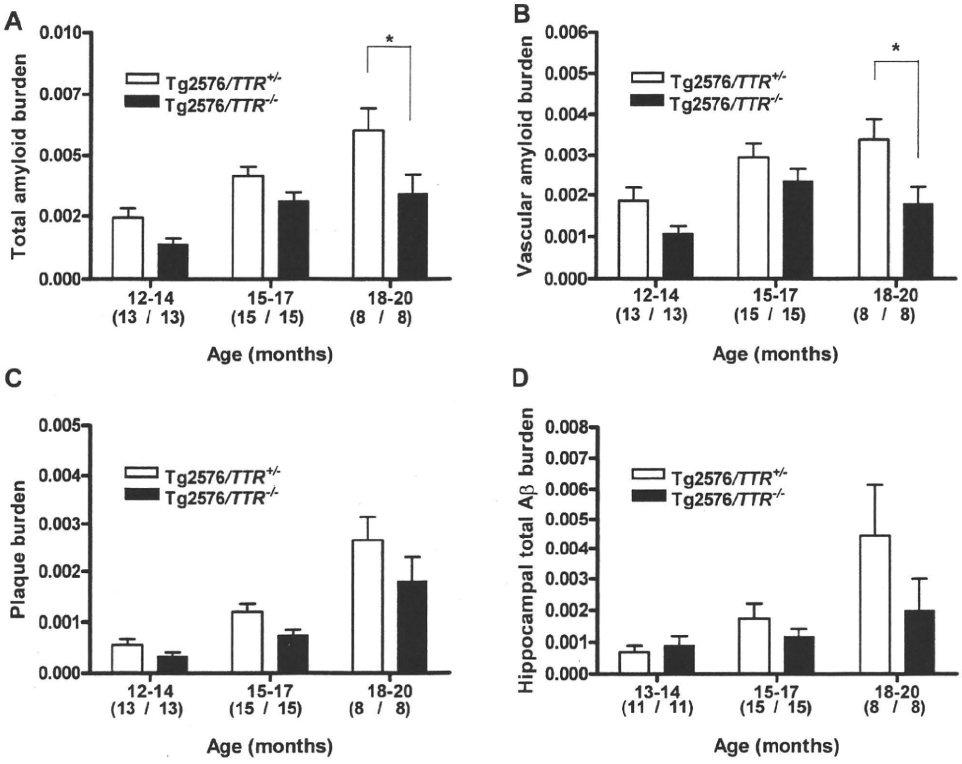

Figure 2. *The Aβ burden in the brain of Tg2576/TTR$^{+/-}$ and Tg2576/TTR$^{-/-}$ mice.* The total Aβ burden (vascular amyloid and plaques) (**A**) vascular Aβ burden (**B**) and Aβ plaque burden (**C**) in the entire cerebral cortex were calculated by dividing total area of Aβ deposits by total area of analyzed cortex. The hippocampal total Aβ burden (**D**) was calculated by dividing area of total Aβ deposits (vascular amyloid and plaques) by area of analyzed hippocampus. All data are expressed as mean ± standard error of the mean. Numbers in parentheses denote numbers of mice examined. *$P < 0.05$. TTR = transthyretin.

mice, however, total Aβ burden was significantly reduced relative to the age-matched Tg2576/*TTR*$^{+/-}$ mice ($P < 0.05$) (Figure 2A). Thus, contrary to our expectations, total Aβ burden is not increased, but rather decreased by eliminating TTR in Tg2576 mice.

Vascular Aβ burden

It had been reported that Tg2576 mice developed abundant vascular amyloid while aging, especially in leptomeningeal vessels (31). In order to determine whether the onset and degree of particular form of Aβ deposition were affected by TTR, we separately assessed vascular amyloid and plaque burdens in the brain of Tg2576/*TTR*$^{+/-}$ and Tg2576/*TTR*$^{-/-}$ mice, as described under *Methods*.

A time-course analysis of vascular Aβ burden was performed by assessing the mice of ages 7–20 months. A few vascular Aβ deposits were first observed at 12 months of age in both Tg2576/*TTR*$^{+/-}$ and Tg2576/*TTR*$^{-/-}$ mice. With advancing age, total vascular Aβ burden increased in both the mice (Figure 2B). Vascular Aβ deposits were detected only in the wall of leptomeningeal vessels of 12–16-month-old Tg2576/*TTR*$^{+/-}$ and Tg2576/*TTR*$^{-/-}$ mice, while in the 17–20-month-old Tg2576/*TTR*$^{+/-}$ and Tg2576/*TTR*$^{-/-}$ mice, the deposits were detected in the vascular wall of cerebral parenchyma as well as the wall of leptomeningeal vessels (data not shown). There was no significant difference in the onset, progression and distribution of vascular Aβ deposition in the entire cerebral cortex between Tg2576/*TTR*$^{+/-}$ and Tg2576/*TTR*$^{-/-}$ mice up to 17 months of age. However, a significant reduction in vascular Aβ burden by 47.1% was found in 18–20-month-old Tg2576/*TTR*$^{-/-}$ mice relative to the age-matched Tg2576/*TTR*$^{+/-}$ mice ($P < 0.05$) (Figure 2B). These findings suggested that TTR does not decrease but rather increases the degree of vascular Aβ burden in Tg2576 mice.

Amyloid-β plaque burden

Aβ plaques were first detected in both Tg2576/*TTR*$^{+/-}$ and Tg2576/*TTR*$^{-/-}$ mice at 12 months of age, and both the size and number of the plaques increased with advancing age (Figure 2C). Although there was a trend to reduction of total Aβ plaque burden in 12–20-month-old Tg2576/*TTR*$^{-/-}$ mice relative to the age-matched Tg2576/*TTR*$^{+/-}$ mice, there was no statistically significant difference in the onset, degree and distribution of Aβ plaque deposition between Tg2576/*TTR*$^{+/-}$ and Tg2576/*TTR*$^{-/-}$ mice (Figure 2C). These findings suggested that TTR does not decrease Aβ plaque burden in the brain of Tg2576 mice.

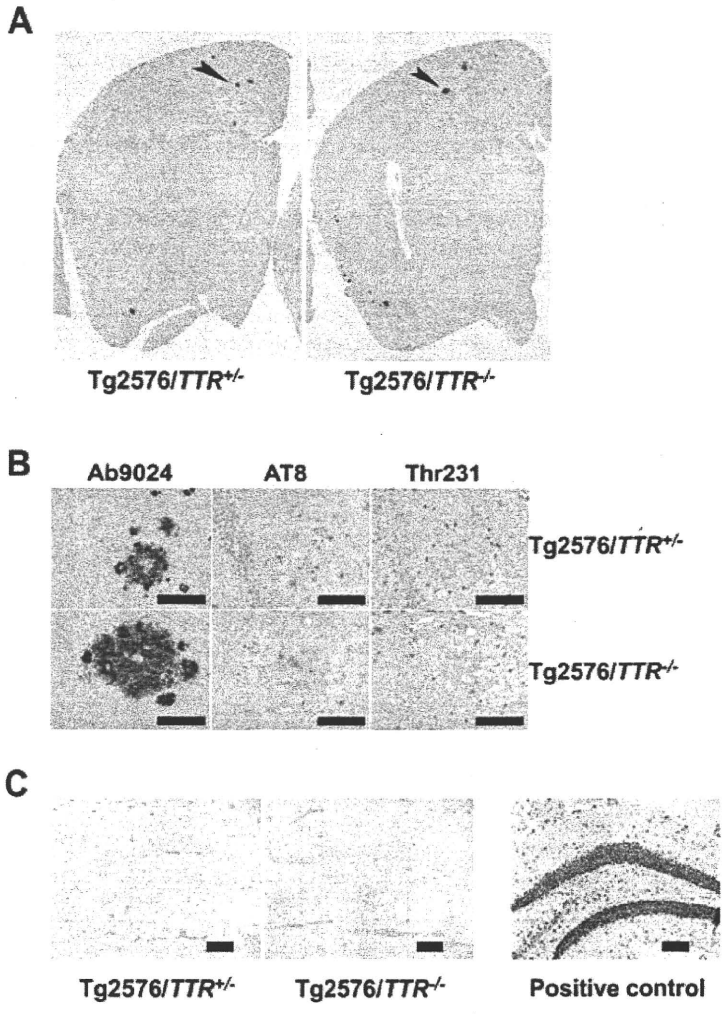

Figure 3. *Immunohistochemistry of Tg2576/TTR$^{+/-}$ and Tg2576/TTR$^{-/-}$ brains.* Immuno-labeling of left hemi-brain sections of 18-month-old Tg2576/*TTR*$^{+/-}$ and Tg2576/*TTR*$^{-/-}$ mice with Ab9204. **A.** The higher magnification of the hippocampal Aβ plaque with giant cores indicated by an arrowhead in **A** (**B**, *left panels*). Serial sections (5 μm) were labeled with AT8, and anti-phosphorylated tau (Thr231). AT8 and Thr-231 labeled punctate dystrophic neurites in and around Aβ plaques (**B**, *middle and right panels, respectively*). Scale bar; 50 μm. The hippocampal dentate gyrus areas of 18-month-old Tg2576/*TTR*$^{+/-}$ and Tg2576/*TTR*$^{-/-}$ mice stained with transferase-mediated dUTP nick end labeling. **C.** No apoptotic cells were found in the hippocampus. A DNaseI-treated sample was stained in parallel with the samples as a positive control. Scale bar; 100 μm. TTR = transthyretin.

Transthyretin deficiency does not affect Aβ deposition in the hippocampus of Tg2576 mice

The hippocampus is highly susceptible area to Aβ deposition in both humans (5) and Tg2576 mice (15). To investigate the effect of TTR deficiency on Aβ deposition in the hippocampus, we measured the total Aβ burden in the hippocampus of Tg2576/*TTR*$^{+/-}$ and Tg2576/*TTR*$^{-/-}$ mice. The Aβ deposits were first detected in the hippocampus of both the mice at 13 months of age, and showed an age-related increase (Figure 2D). Although the total Aβ burden in Tg2576/*TTR*$^{+/-}$ mice was consistently greater than that in Tg2576/*TTR*$^{-/-}$ mice, the difference was not statistically significant. Thus, the TTR deficiency does not affect Aβ deposition in the hippocampus of Tg2576 mice.

Transthyretin deficiency does not increase but decreases the level of Aβ40 in the brain of Tg2576 mice

Different forms of Aβ, biochemically distinguishable by their solubility properties, are present in varying amounts during the lifetime of Tg2576 mice. Detergent-soluble Aβ (SDS fraction) is present throughout life; however, detergent-insoluble Aβ (FA fraction) is absent up to age 6 months (18). It had been reported in AD that the predominant Aβ peptide present in CAA is Aβ40; however, in brain parenchymal plaques, it is Aβ42 (1, 7, 17, 29, 44). To evaluate whether or not TTR affects the level of different forms of Aβ, we quantified the Aβ40 and Aβ42 in SDS and FA fractions of brain homogenates from Tg2576/*TTR*$^{+/-}$ and Tg2576/*TTR*$^{-/-}$ mice by sandwich ELISA, as described under *Methods*. The number and age of 13–20-month-old Tg2576/*TTR*$^{+/-}$ and Tg2576/*TTR*$^{-/-}$ mice examined were shown in Table 2. Aβ40 and Aβ42 levels in SDS and FA fractions increased with age in both the mice. There was no significant difference in the levels of Aβ40 and Aβ42 in both the fractions between Tg2576/*TTR*$^{+/-}$ and Tg2576/*TTR*$^{-/-}$ mice up to 17 months of age. In 18–20-month-old Tg2576/*TTR*$^{-/-}$ mice, however, the levels of Aβ40 in both SDS and FA fractions were significantly reduced by 35.2% and by 41.6%, respectively, relative to the age-matched Tg2576/*TTR*$^{+/-}$ mice ($P < 0.05$) (Figure 4A,B). The level of Aβ42 in SDS fraction was also significantly reduced by 57.8% in 18–20-month-old